*Endocrinology*, 2021, Vol. 162, No. 6, 1–20
doi:10.1210/endocr/bqab064
Research Article

Research Article

# CX3CL1-CX3CR1 Signaling Deficiency Exacerbates Obesity-induced Inflammation and Insulin Resistance in Male Mice

**Mayumi Nagashimada,[1,2] Kazuki Sawamoto,[1] Yinhua Ni,[1,3] Hironori Kitade,[1] Naoto Nagata,[1] Liang Xu,[1] Masuko Kobori,[4] Naofumi Mukaida,[5] Tatsuya Yamashita,[1] Shuichi Kaneko,[1] and Tsuguhito Ota[1]**

[1]Advanced Preventive Medical Sciences Research Center, Kanazawa University, Kanazawa, Japan; [2]Division of Health Sciences, Graduate School of Medical Science, Kanazawa University, Kanazawa, Japan; [3]College of Biological Engineering, Zhejiang University of Technology, Hangzhou, China; [4]Food Research Institute, National Agriculture and Food Research Organization, Tsukuba, Japan; and [5]Division of Molecular Bioregulation, Cancer Research Institute, Kanazawa University, Kanazawa, Japan

**ORCiD number:** 0000-0003-2714-6395 (M. Nagashimada).

**Abbreviations:** ATM, adipose tissue macrophage; CCR2, C-C chemokine receptor 2; FACS, fluorescence-activated cell sorting; GTT, glucose tolerance test; H&E, hematoxylin and eosin; IL, interleukin; IRβ, insulin receptor β-subunit; LPS, lipopolysaccharide; MAPK, mitogen-activated protein kinase; NF-κB, nuclear factor κB; SVF, stromal vascular fraction; TC, total cholesterol; TG, triglycerides; Tnf, tumor necrosis factor; WAT, white adipose tissue

Received: 2 December 2020; Editorial Decision: 20 March 2021; First Published Online: 25 March 2021; Corrected and Typeset: 22 May 2021.

## Abstract

The CX3CL1-CX3CR1 system plays an important role in disease progression by regulating inflammation both positively and negatively. We reported previously that C-C chemokine receptors 2 and 5 promote obesity-associated adipose tissue inflammation and insulin resistance. Here, we demonstrate that CX3CL1-CX3CR1 signaling is involved in adipose tissue inflammation and insulin resistance in obese mice via adipose tissue macrophage recruitment and M1/M2 polarization. *Cx3cl1* expression was persistently decreased in the epididymal white adipose tissue (eWAT) of high-fat diet-induced obese (DIO) mice, despite increased expression of other chemokines. Interestingly, in *Cx3cr1*$^{-/-}$ mice, glucose tolerance, insulin resistance, and hepatic steatosis induced by DIO or leptin deficiency were exacerbated. CX3CL1-CX3CR1 signaling deficiency resulted in reduced M2-polarized macrophage migration and an M1-dominant shift of macrophages within eWAT. Furthermore, transplantation of *Cx3cr1*$^{-/-}$ bone marrow was sufficient to impair glucose tolerance, insulin sensitivity, and regulation of M1/M2 status. Moreover, Cx3cl1 administration in vivo led to the attenuation of glucose intolerance and insulin resistance. Thus, therapy targeting the CX3CL1-CX3CR1 system may be beneficial in the treatment of type 2 diabetes by regulating M1/M2 macrophages.

**Key Words:** chemokine, obesity, insulin resistance, inflammation, macrophage polarization

ISSN Online 1945-7170

Obesity is a state of chronic low-grade inflammation. It has been reported that chronic inflammation is closely related to increase proinflammatory cytokines and chemokines. Especially, the accumulation of adipose tissue macrophages (ATMs) through C-C chemokine receptor 2 (CCR2) and its ligand CCL2 (also known as monocyte chemoattractant protein 1) is considered to be pivotal in the development of obesity-induced inflammation and insulin resistance (1-4). In addition, we reported previously that a different chemokine receptor, CCR5, promoted obesity-associated adipose tissue inflammation and insulin resistance (5, 6).

In the present study, we found that the expression of CX3CL1 was persistently decreased in epididymal white adipose tissue (eWAT). CX3CL1 (also known as fractalkine) is a CX3C chemokine involved in cell adhesion, recruitment, and survival through binding to the G protein-coupled receptor CX3CR1 (7-10). There is accumulating evidence that the CX3CL1-CX3CR1 system exerts both negative and positive effects on the pathogenesis and progression of different diseases. Highly enhanced CX3CL1-CX3CR1 signaling could induce inflammation in atherosclerosis (11-13), cardiovascular disease (14), and rheumatoid arthritis (15, 16) through the regulation of inflammatory macrophages and T lymphocytes. In addition, $CX3CR1^{+}$ monocytes can differentiate into activated macrophages in many tissues (17). In contrast, enhancement of CX3CL1-CX3CR1 signaling had preventive effects on intestinal inflammation and colitis (18, 19), pancreatic β cell dysfunction (20), and diet-induced obesity (21). Furthermore, CX3CL1-CX3CR1 signaling during macrophage polarization induced accumulation of M2-like macrophages in skin cancer (22). However, the effects of the CX3CL1-CX3CR1 axis on ATM polarization, adipose inflammation, and insulin resistance on the development of obesity are still not clear.

Here, we show that loss of CX3CL1-CX3CR1 signaling exacerbates insulin resistance and inflammation in high-fat (HF) diet-induced obese (DIO) mice by causing a decrease in the number of anti-inflammatory M2-like macrophages and an increase in the number of proinflammatory M1-like macrophages. Importantly, administration of CX3CL1 improved glucose tolerance and insulin resistance in DIO mice, suggesting that the CX3CL1-CX3CR1 system may be a novel target for the treatment of obesity-induced type 2 diabetes.

## Materials and Methods

### Mouse models

C57BL/6J mice were purchased from Charles River Laboratories (Yokohama, Japan). *Cx3cr1*$^{-/-}$ mice and *Ccl2*$^{-/-}$ mice were kindly provided by N. Mukaida (Kanazawa University, Ishikawa, Japan). The mice were generated as reported previously (11, 12, 23). C57BL/6J mice and *Cx3cr1*$^{-/-}$ mice were fed normal chow (NC), in which 10% of calories were from fat (CRF-1; Charles River Laboratories), or an HF diet consisting of 60% fat (Research Diets, New Brunswick, NJ, USA). We compared *Cx3cr1*$^{-/-}$ mice and their wild-type (WT) littermates. All mice were maintained under a 12 h/12 h light/dark cycle and given free access to food and water. All mice were males with a C57BL/6 background. The glucose tolerance test (GTT) was conducted after an overnight fast, and the mice were then injected intraperitoneally (ip) with 2 g/kg glucose. The insulin tolerance test was performed after a 4 h fast; mice were injected ip with 0.5 U/kg insulin. All experiments and animal procedures were performed in accordance with the standards set forth in the Guidelines for the Care and Use of Laboratory Animals and were approved by the Gene Recombination Experiment Safety Committee and the Institute for Experimental Animal Committee of Kanazawa University.

### Cell culture experiments

Peritoneal macrophages were isolated and cultured as described previously (24). Eight-week-old male WT and *Cx3cr1*$^{-/-}$ mice were injected with 4% (w/v) thioglycolate. Peritoneal macrophages were isolated 48 h later and cultured in Dulbecco's modified Eagle's medium (Gibco Invitrogen, Carlsbad, CA, USA) supplemented with 10% (v/v) fetal bovine serum. After 6 h of starvation, cells were incubated with lipopolysaccharide (LPS; Sigma-Aldrich, St. Louis, MO, USA) at 1, 10, 100, or 1000 ng/mL or with interleukin 4 (IL-4; R&D Systems) at 1, 10, or 100 ng/mL for 16 h in 6-well plates at 37°C under 5% (v/v) $CO_2$.

### DNA microarray analysis

Total RNA was extracted from eWAT using an messenger RNA (mRNA) Miniprep Kit (Roche, Basel, Switzerland). Fragmented biotin-labeled complimentary RNA was synthesized from the total RNA of each mouse using a GeneChip 3 IVT Express Kit (Affymetrix Japan KK, Tokyo, Japan) and then hybridized to a GeneChip Mouse Genome 430 2.0 array (Affymetrix). After hybridization, the probe array was stained using the GeneChip Fluidics Station 450 (Affymetrix) and then scanned using the GeneChip Scanner 3000 instrument (Affymetrix) and GeneChip Operation Software (ver. 1.4; Affymetrix). Analysis of DNA microarray data was performed using Microarray Suite 5.0 (Affymetrix) and GeneSpring (v. 11.5; Agilent Technologies, Santa Clara, CA, USA). The data are accessible through Gene Expression

Omnibus Series accession number GSE167311 (https://www.ncbi.nlm.nih.gov/geo/query/acc.cgi?acc=GSE167311).

## Quantitative real-time polymerase chain reaction

Quantitative real-time polymerase chain reaction (PCR) was performed as described previously (5, 25). Total RNA was extracted from frozen adipose tissue and other tissues using a High Pure RNA Tissue Kit (Roche). Complimentary DNA (cDNA) was synthesized from total RNA using a High Capacity cDNA Synthesis Kit (Applied Biosystems, Foster City, CA, USA). Quantitative real-time PCR was performed on a CFX384 Touch Real-Time PCR Detection System (Bio-Rad, Hercules, CA, USA) using SYBR Select Master Mix (Thermo Fisher Scientific, Waltham, MA, USA). Standard curves were generated for relative quantification of specific PCR products for each primer set (Table 1). mRNA levels were normalized relative to the amount of 18S rRNA and expressed in arbitrary units. Levels of S18 transcript were used for normalization.

## Plasma protein measurements

Plasma triglycerides (TG), total cholesterol (TC), nonesterified fatty acid, glucose, insulin levels (26), and hepatic TG levels were measured as described previously (5, 25). Plasma fractalkine (R&D Systems) (27) and TNF-α (Thermo Fisher Scientific) (28) levels were measured by enzyme-linked immunosorbent assay.

## Immunoblotting

Total tissues were homogenized and sonicated in radio immunoprecipitation assay lysis buffer (Millipore, Bedford, MA, USA) supplemented with protease inhibitors and PhosStop (Roche). Proteins were separated by sodium dodecyl sulfate-polyacrylamide gel electrophoresis, transferred onto polyvinylidene fluoride or polyvinylidene difluoride membranes (Millipore) and probed with anti-phospho (p)-p38 mitogen-activated protein kinase (MAPK) (29), anti-p38 MAPK (30), anti-p-nuclear factor κB (NF-κB) p65 (31), anti-NF-κB (32), anti-p-Tyr1146 insulin receptor β subunit (IRβ) (33), anti-IRβ (34), anti-p-protein kinase B (Akt) (35), anti-Akt (cell signaling) (36), and monoclonal anti-β-actin (Sigma-Aldrich) (37) antibodies.

## Histological analysis

Paraffin-embedded eWAT, liver, and pancreatic tissue sections were stained with hematoxylin and eosin and immunohistochemically stained for F4/80 (Abcam, Cambridge, UK) (38), insulin (Abcam) (39), glucagon (Sigma-Aldrich) (40), Ki67 (Abcam) (41), and 4′,6-diamidino-2-phenylindole (Dojindo). The macrophage area was measured in 5 randomly selected fields at 200× magnification for each mouse ($n$ = 4-6 mice per group). Relative β cell areas were calculated by dividing the area of insulin-positive cells by the total pancreatic area measured using an AxioVision system (Carl Zeiss, Dublin, CA, USA) ($n$ = 3-5 mice per group).

Whole-mount immunostaining of eWAT was performed as described previously (42). Mice were perfused with 1% paraformaldehyde, and the eWAT was dissected out and stained with rat antimouse F4/80 (Abcam), rabbit anti-CX3CR1 (Abcam) (43), rabbit anti-CX3CL1 (Torrey Pines Biolabs, Secaucus, NJ, USA) (44), rat anti-CD206 (Bio-Rad) (45), hamster anti-CD11c (Bio-Rad) (46), and guinea pig antiperilipin

**Table 1.** Primer sequence for quantitative real-time polymerase chain reaction

| Gene | 5’ Primer | 3’ Primer |
|---|---|---|
| *mCx3cr1* | CCG CCA ACT CCA TGA ACA A | CGT CTG GAT GAT GCG GAA GTA |
| *mCx3cl1* | CAC CTC GGC ATG ACG AAA T | TTG TCCA CCC GCT TCT CAA |
| *mCcl2* | AGG TCC CTG TCA TGC TTC TGG | CTG CTG CTG GTG ATC CTC TTG |
| *mCcr2* | ATT CTC CAC ACC CTG TTT CG | GAT TCC TGG AAG GTG GTC AA |
| *mAdgre1* | CTT TGG CTA TGG GCT TCC AGT C | GCA AGG AGG ACA GAG TTT ATC GTG |
| *mTnf* | AAG CCT GTA GCC CAC GTC GTA | GGC ACC ACT AGT TGG TTG TCT TTG |
| *mIl1b* | CTG AAC TCA ACT GTG AAA TGC CA | AAA GGT TTG GAA GCA GCC CT |
| *mIl10* | GCT CTT ACT GAC TGG CAT GAG | CGC AGC TCT AGG AGC ATG TG |
| *mMrc1* | CAA GGA AGG TTG GCA TTT GT | CCT TTC AGT CCT TTG CAA GC |
| *mMgl1* | TGA GAA AGG CTT TAA GAA CTG GG | GAC CAC CTG TAG TGA TGT GGG |
| *mItgax* | AAA ATC TCC AAC CCA TGC TG | CAC CAC CAG GGT CTT CAA GT |
| *mNos2* | AAT CTT GGA GCG AGT TGT GG | CAG GAA GTA GGT GAG GGC TTG |
| *mLeptin* | AAG AAG ATC CCA GGG AGG AA | TGA TGA GGG TTT TGG TGT CA |
| *mAdiponectin* | AGC CGC TTA TAT GTA TCG CTC A | TGC CGT CAT AAT GAT TCT GTT GG |
| *18SrRNA* | GGA GAA CTC ACG GAG GAC GA | CCA GTG GTC TTG GTG TGC TG |

(Fitzgerald Industries International, Concord, MA, USA) (47) antibodies overnight at 4°C. To detect signals, appropriate secondary antibodies conjugated with Alexa Fluor 488 (48-50) or Alexa Fluor 594 (51-53) (Jackson ImmunoResearch Laboratories, Thermo Fisher Scientific) were used. Samples were visualized under an inverted confocal microscope using an LSM5 PASCAL system (Carl Zeiss).

### Isolation of adipocytes and stromal vascular fraction cells

Epididymal fat pads from male C57BL/6J mice fed the NC or HF diet were minced with scissors and digested for 20 min at 37°C with type II collagenase (Sigma-Aldrich) in PBS containing 2% BSA (pH 7.4). The cell suspension was filtered through a 100-µm filter and then centrifuged at 300 × *g* for 5 min to separate the floating adipocyte fraction from the SVF cells. Both fractions were used for RNA extraction or flow cytometric analysis.

### Flow cytometric analysis

SVF cells were resuspended in PBS supplemented with 2% fetal bovine serum and incubated with Fc-Block (BD Biosciences, Franklin Lakes, NJ, USA), followed by incubation with fluorochrome-conjugated antibodies as described previously (5, 54, 55). Cells were analyzed using FACSAria II (BD Biosciences), and data were acquired with FACSDiva software (version 6.0; BD Biosciences). Data analysis was performed using FlowJo software (Tomy Digital Biology, Tokyo, Japan). Unstained, single stained, and fluorescence minus 1 controls were used to set compensation and gates. Polyimide was used to identify live cells.

### GTT and insulin tolerance test

The GTT was performed after an overnight fast. After baseline blood collection, mice were injected ip with glucose (2 g/kg body weight). Blood samples were collected 15, 30, 60, 90, 120, and 180 min later for determination of glucose and insulin levels. The insulin tolerance test was performed after a 4 h fast. Mice were injected ip with human insulin (0.75 U/kg for HF-diet-fed mice and 1.5 U/kg for *Cx3cr1/ob* and *ob/ob* littermates). All blood samples were collected by cutting the tail 1 to 2 mm from the tip with sharp scissors. The blood glucose level was measured using glucose test strips and a glucose enzyme-linked immunosorbent assay kit (FUJIFILM Wako Pure Chemical, Osaka, Japan) as described previously (24, 25).

### Bone marrow transplantation

Bone marrow cells were collected from the femurs and tibias of 8-week-old *Cx3cr1*$^{-/-}$ or C57BL/6J (WT) mice and transplanted via the tail vein into lethally irradiated (10 Gy) recipient WT mice with a minimum cell dose of $10^7$ cells. The following groups of chimeric mice were generated: WT to WT, *Cx3cr1*$^{-/-}$ to WT, WT to *Cx3cr1*$^{-/-}$, and *Cx3cr1*$^{-/-}$ to *Cx3cr1*$^{-/-}$. Transplanted mice could recover for 4 weeks to reconstitute their hematopoietic systems. Genomic DNA was extracted from peripheral blood. Mice were then placed on the NC or HF diet for 8 weeks and the GTT was performed. Tissues were harvested after 10 weeks of feeding on the specified diet.

### Effects of CX3CL1 treatment on diet-induced obesity

Full-length CX3CL1 cDNA was obtained from mouse liver tissue by PCR. CX3CL1 cDNA was cloned into the pLIVE vector (Mirus Bio, Madison, WI, USA). The control vector was pLIVE vector without any insert. After feeding with the HF diet for 6 weeks, C57BL/6J and *Cx3cr1*$^{-/-}$ mice were injected with either pLIVE-CX3CL1 or control vector at a dose of 10 µg/mouse suspended in 2 mL of TransIT-EE Hydrodynamic Delivery Solution (Mirus Bio) (56).

### Statistics

All data are presented as means ± standard error of the mean (SEM). Comparisons between 2 groups were performed using the 2-tailed Student's *t*-test. All analyses were performed using IBM SPSS Statistics (version 24; IBM Corp., Armonk, NY, USA). The gene expression levels obtained by DNA microarray analysis were compared among mouse groups using Welch's 1-way analysis of variance followed by Tukey's post-hoc test with Benjamini-Hochberg adjustment for multiple corrections. Genes that were significantly differentially expressed between 2 groups were further analyzed by Ingenuity Pathway Analysis (Ingenuity Systems, Redwood, CA, USA).

## Results

### Cx3cl1 expression is downregulated in the adipose tissue of obese mice

We first compared the gene expression of various chemokines and their receptors between the eWAT of DIO mice and lean mice fed NC using DNA microarray analysis. Consistent with previous studies, monocyte chemoattractant protein 1-CCR2 and CCL5-CCR5 signaling were enhanced during the development of obesity (Fig. 1A).

Surprisingly, we found that the expression of *Cx3cl1* was decreased in the eWAT of DIO mice (Fig. 1A). In addition, real-time PCR analysis confirmed that *Cx3cl1* mRNA was downregulated only in eWAT and not in other tissues of DIO mice (Fig. 1B). The mRNA levels of *Ccl2* and its receptor, *Ccr2*, were increased in eWAT between 8 and 20 weeks after starting the HF diet and in *ob/ob* mice at 8 weeks old. Interestingly, *Cx3cl1* expression continued to decline during HF feeding and decreased markedly in *ob/ob* mice at 8 weeks of age, while *Cx3cr1* expression showed no significant difference (Fig. 1C and 1D). Furthermore, the plasma *Cx3cl1* concentration was significantly reduced in DIO mice compared with lean mice (Fig. 1E). We next investigated the cellular sources of *Cx3cl1* and *Cx3cr1* gene expression in the eWAT of DIO and lean mice. The mRNA levels of *Cx3cl1* and *Cx3cr1* in adipocytes and a macrophage-containing stromal vascular fraction (SVF) of eWAT were determined using real-time PCR. *Cx3cl1* and *Cx3cr1* expression was higher in the SVF than in the adipocyte fraction in DIO and lean mice (Fig. 1F). Moreover, *Cx3cl1* expression in SVF was markedly decreased after starting the HF diet. Immunostaining revealed that Cx3cr1 and Cx3cl1 were expressed mainly in F4/80$^+$ macrophages, and not in perilipin$^+$ adipocytes. Moreover, both Cx3cr1 and Cx3cl1 were expressed in CD11c$^+$CD206$^-$ M1-like ATMs and CD11c$^-$CD206$^+$ M2-like ATMs (Fig. 1G). Together, the results showed that the expression of Cx3cl1 was downregulated in the eWAT of obese mice.

## Deficiency of CX3CL1-CX3CR1 signaling exacerbates diet-induced insulin resistance, hepatic steatosis, and adipose tissue inflammation

To clarify the impact of CX3CL1-CX3CR1 signaling on obesity-induced insulin resistance and inflammation in vivo, we analyzed the metabolic phenotype in WT and *Cx3cr1*$^{-/-}$ mice fed the NC or HF diet for 16 weeks. WT and *Cx3cr1*$^{-/-}$ mice showed similar weight gain (Fig. 2A). Our findings indicated that sex had no effect on body weight gain in *Cx3cr1*$^{-/-}$ mice on the HF diet (data not shown). Adipose tissue weight, liver weight, and fasting plasma glucose levels were not significantly different between *Cx3cr1*$^{-/-}$ and WT mice maintained on either the NC or HF diet (Table 2). Plasma TG, TC, and nonesterified fatty acid levels tended to increase in *Cx3cr1*$^{-/-}$ mice on either the NC or HF diet compared with WT controls (Table 2). Hepatic TG accumulation was increased in *Cx3cr1*$^{-/-}$ mice on the HF diet (Fig. 2B). The GTT indicated impaired glucose tolerance in lean and obese *Cx3cr1*$^{-/-}$ mice compared with WT mice (Fig. 2C and 2D). Moreover, HF diet-induced hyperinsulinemia was significantly exacerbated in *Cx3cr1*$^{-/-}$ mice (Fig. 2E). *Cx3cr1*$^{-/-}$ mice showed marked increases in F4/80$^+$ macrophage infiltration into adipose tissue and crown-like structure formation induced by the HF diet (Fig. 2F, 2G, and 2I). However, there was no significant difference in adipocyte size between *Cx3cr1*$^{-/-}$ and WT mice (Fig. 2H). Obese *Cx3cr1*$^{-/-}$ mice had significantly increased expression of *leptin*, while there was no significant differences in *adiponectin* gene expression (Fig. 2I). These findings were associated with augmented NF-κB p65 phosphorylation in *Cx3cr1*$^{-/-}$ mice on the HF diet (Fig. 2J). Importantly, the gene expression levels of the M1 macrophage marker, *Itgax*, and inflammatory cytokine, *Tnf*, were higher in *Cx3cr1*$^{-/-}$ mice than in WT mice on the NC or HF diet (Fig. 2I), but there was no difference in expression of the M2 macrophage marker, *Mrc1* (Fig. 2I). In addition, plasma levels of TNF-α were significantly higher in *Cx3cr1*$^{-/-}$ mice than in WT mice fed the HF diet (Fig. 2K). Moreover, insulin-stimulated tyrosine phosphorylation of insulin receptor β subunit (p-IRβ) and Akt (p-Akt) was decreased in the liver and eWAT of *Cx3cr1*$^{-/-}$ mice compared with WT mice (Fig. 2L).

To examine the effects of CX3CR1 deficiency on β cell mass, we measured the size of insulin-positive islet cells by morphometric analysis. The islet size increased in both WT and *Cx3cr1*$^{-/-}$ mice on the HF diet. However, there was no significant difference in β cell mass or proliferation between WT and *Cx3cr1*$^{-/-}$ mice on the same diet (Fig. 3A-3D). The size of glucagon-positive α cells in *Cx3cr1*$^{-/-}$ mice was also unaffected.

## CX3CL1-CX3CR1 signaling causes a reciprocal increase in M1-like ATMs and decrease in M2-like ATMs

Next, macrophage infiltration and polarization were assessed. The infiltration of CD11c$^+$CD206$^-$ (M1-like) ATMs was increased in *Cx3cr1*$^{-/-}$ mice compared with WT mice on either the NC or HF diet (Fig. 4A). We then examined the distributions of Cx3cl1 and Cx3cr1 in ATMs from DIO mice by immunofluorescence analysis and found that both M1-like and CD11c$^-$CD206$^+$ (M2-like) ATMs expressed Cx3cl1 and Cx3cr1 (Fig. 4A).

To quantify ATM subsets in WT and *Cx3cr1*$^{-/-}$ mice on the NC or HF diet, we performed flow cytometric analysis. *Cx3cr1*$^{-/-}$ mice fed the NC diet showed a 40.3% increase in M1-like macrophages and 17% decrease in M2-like macrophages compared with WT mice (Fig. 4B and 4D). Moreover, *Cx3cr1*$^{-/-}$ mice on the HF diet had 39% more M1-like macrophages and 49% fewer M2-like macrophages than WT mice (Fig. 4C and 4E), which resulted in a predominance of M1 over M2 in the ATM population (Fig. 4D and

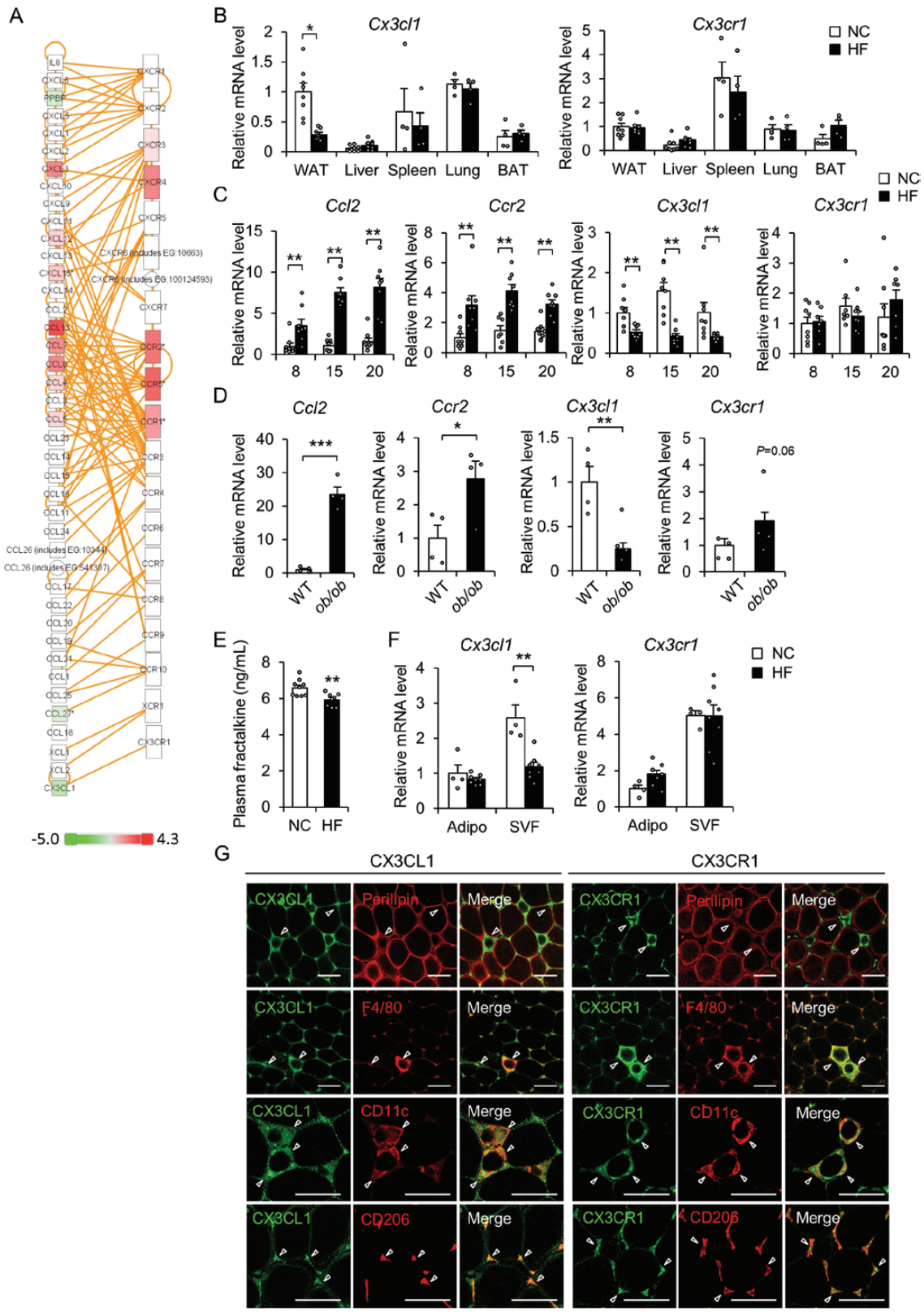


**Figure 1.** Cx3cl1 is downregulated in the eWAT of obese mice. (A) Changes in gene expression of chemokines and their receptors in the adipose tissue of WT fed the NC or HF diet for 8 weeks. Upregulated (red) and downregulated (green) genes in comparison with WT were detected by DNA microarray analysis ($n = 5$ per group). (B) Gene expression of *Cx3cl1* and its receptor *Cx3cr1* in various tissues of WT and DIO mice at 20 weeks old ($n = 4$-8 per group). (C and D) mRNA expression of receptors and their ligands in the adipose tissue of WT and DIO mice at 8, 15, and 20 weeks old and *ob/ob* mice at 8 weeks old ($n = 4$ per group). (E) Plasma Cx3cl1 protein levels were measured at 16 weeks old ($n = 8$ per group). (F) mRNA expression

4E). On the other hand, the total number of ATMs was not different between genotypes on the same diet (Fig. 4D and 4E). Furthermore, a predominance of lymphocyte antigen 6C (Ly6C)$^{hi}$ over the Ly6C$^{-}$ monocyte population was also observed in both the peripheral blood and bone marrow cells of *Cx3cr1*$^{-/-}$ mice (Fig. 4F-4J). In parallel, *Cx3cr1* deficiency increased the mRNA expression of LPS-induced M1 markers, such as *Tnf* and *Il1b*, in peritoneal macrophages, whereas *Cx3cr1* deficiency decreased the mRNA expression of IL-4-induced M2 markers, such as *Mrc1* and *Il10* (Fig. 5A). Cx3cl1 alone had no effect on the expression of macrophage markers, but exposure of peritoneal macrophages to Cx3cl1 decreased the expression of LPS-induced M1 macrophage markers in a dose-dependent manner. Moreover, exposure of macrophages to Cx3cl1 increased the mRNA expression of M2 macrophage markers in the presence of IL-4 (Fig. 5B). Therefore, loss of CX3CL1-CX3CR1 signaling in macrophages resulted in a shift in polarization toward an inflammatory phenotype.

## Transplantation of *Cx3cr1*$^{-/-}$ bone marrow promoted metabolic dysfunction in mice

To further study the impact of CX3CR1 deficiency in bone marrow-derived macrophages, we transplanted bone marrow cells from age-matched WT or *Cx3cr1*$^{-/-}$ mice into lethally irradiated WT mice, to generate myeloid cell-specific chimeric mice. To detect *Cx3cr1*$^{-/-}$ cells in the blood of chimeric mice, which have loss of Cx3cr1 only in myeloid cells (*Cx3cr1*$^{-/-}$ to WT), we performed PCR on genomic DNA from whole blood with primers specific for the deletion mutant *neo* gene in the *Cx3cr1* targeting vector. The *neo* amplification product was not detected in samples of bone marrow transplanted from WT into WT (WT to WT) mice, but was present in all of the samples of bone marrow transplanted from *Cx3cr1*$^{-/-}$ to WT mice (Fig. 6A).

To study the effects of the CX3CL1-CX3CR1 pathway in bone marrow-derived macrophages on glucose metabolism, WT to WT and *Cx3cr1*$^{-/-}$ to WT mice were fed the HF diet for 12 weeks. Both groups of transplant recipient mice gained weight and developed a similarly moderate level of DIO (Fig. 6B). Bone marrow transplanted from *Cx3cr1*$^{-/-}$ to WT mice exacerbated HF diet-induced hepatic steatosis (Fig. 6C), impaired glucose tolerance (Fig. 6D), and reduced insulin signaling (Fig. 6E), but did not affect macrophage infiltration into eWAT (Fig. 6F). These results suggested that the transfer of *Cx3cr1*$^{-/-}$ hematopoietic cells was sufficient to promote diet-induced alterations in glucose metabolism. However, lacking Cx3cr1 only in myeloid cells caused a 30% increase in M1-like macrophages and 16.7% decrease in M2-like macrophages compared with WT mice, which resulted in a shift to an M1-like dominant ATM phenotype (Fig. 6G and 6H).

We next assessed the recovery of CX3CL1-CX3CR1 signaling in bone marrow-derived macrophages. We generated WT to *Cx3cr1*$^{-/-}$ (WT to *Cx3cr1*$^{-/-}$) and *Cx3cr1*$^{-/-}$ to *Cx3cr1*$^{-/-}$ (*Cx3cr1*$^{-/-}$ to *Cx3cr1*$^{-/-}$) mice, both of which showed similar weight gain (Fig. 7A). WT to *Cx3cr1*$^{-/-}$ mice had slightly improved glucose tolerance (Fig. 7B). However, there were no differences in M1- or M2-like macrophages between the groups (Fig. 7C and 7D). Thus, CX3CL1-CX3CR1 signaling in bone marrow-derived cells protected against obesity-induced adipose tissue inflammation and glucose intolerance. These observations suggested that macrophage Cx3cr1 propagates the inflammatory response to obesity. The chimeric mice lacked Cx3cr1 only in myeloid cells derived from the bone marrow transplant (BMT).

## CX3CR1 ablation promotes adipose tissue inflammation and insulin resistance in *ob/ob* mice

To further assess the role of CX3CR1 in genetically obese (*ob/ob*) mice, *Cx3cr1* and *leptin*-deficient (*Cx3cr1/ob*) mice were generated by crossing *Cx3cr1*$^{-/-}$ and *ob/ob* mice. *Cx3cr1/ob* mice showed less weight gain than *ob/ob* mice until 8 weeks of age, but the adiposity was similar thereafter (Fig. 8A and 8B). *Cx3cr1/ob* mice developed hepatic steatosis (Fig. 8C and 8D), impaired glucose tolerance (Fig. 8E), and insulin resistance (Fig. 8F). Notably, *Cx3cr1/ob* mice had increased ATM recruitment compared with *ob/ob* littermates, although adipocyte size was similar between the groups (Fig. 8G-8I). Consistent with obese *Cx3cr1*$^{-/-}$ mice, *Cx3cr1/ob* mice had markedly decreased expression of M2 macrophage markers compared with controls (Fig. 8J). Moreover, inflammatory signals were enhanced in the eWAT of *Cx3cr1/ob* mice (Fig. 8K), in association with impaired insulin signaling (Fig. 8L).

**Figure 1: continued**

of *Cx3cl1* and its receptor in the adipocyte fraction and SVF of eWAT of mice ($n$ = 4-8 per group). (G) Immunocytochemical analysis of the epididymal adipose tissue of DIO mice with anti-cx3cl1 (green), anti-cx3cr1 (green), anti-F4/80 (red), anti-perilipin (red), anti-CD11c (red), and anti-CD206 (red) antibodies. Scale bar: 100 μm. Data in (B-E) are expressed as means ± SEM and were analyzed by 2-tailed Student's *t*-test; *$P$ < 0.05, **$P$ < 0.01, ***$P$ < 0.001. Abbreviations: BAT, brown adipose tissue; eWAT, epididymal white adipose tissue.

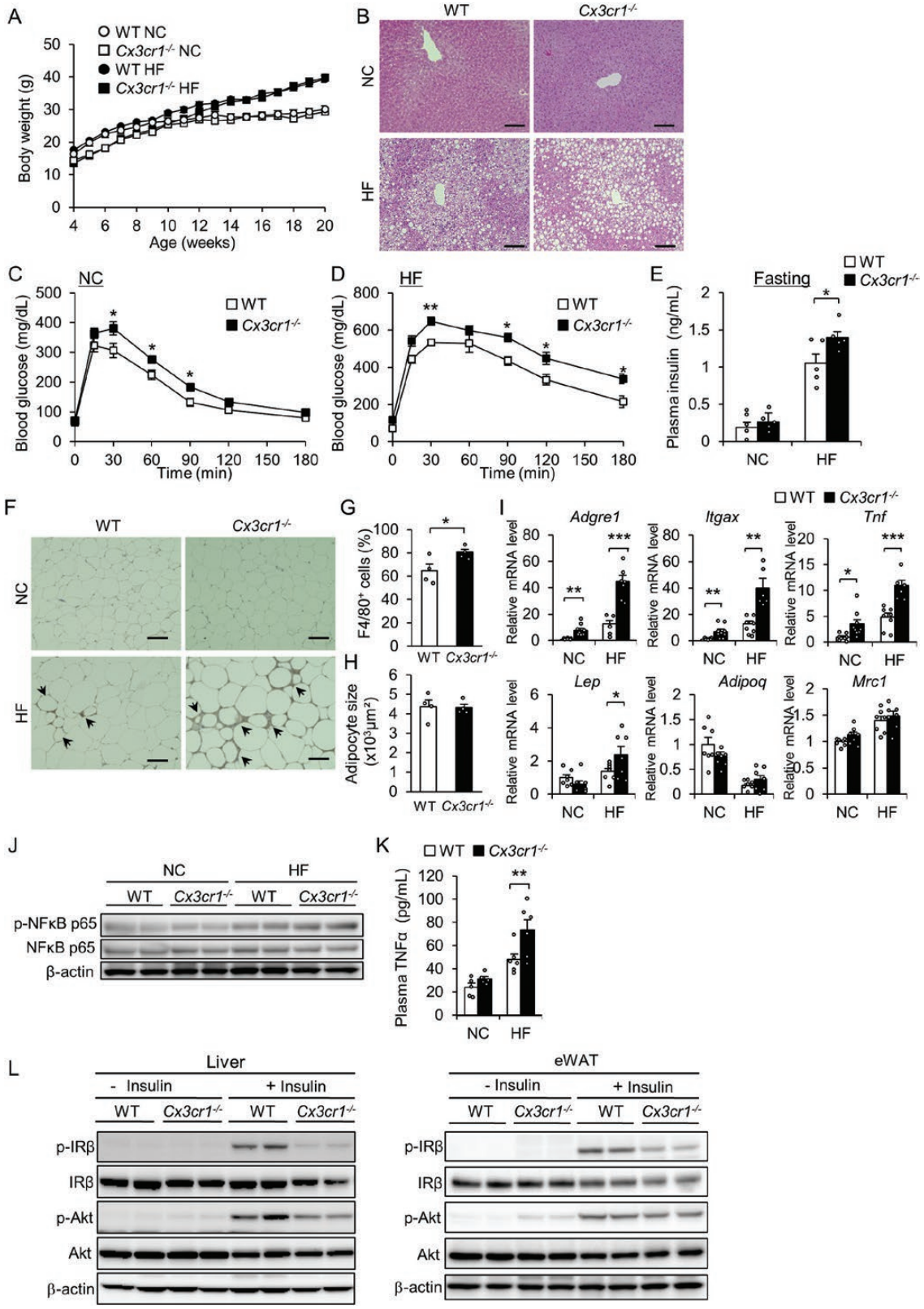


**Figure 2.** Cx3cr1-deficiency promotes diet-induced insulin resistance, hepatic steatosis, and adipose tissue inflammation. (A) Body weights of WT and *Cx3cr1*$^{-/-}$ mice fed the NC or HF diet for 16 weeks ($n = 7$ per group). (B) Representative images of HE-stained liver slices. Scale bar: 100 μm. (C and D) GTT ($n = 7$ per group). (E) Plasma insulin levels in the fasting state ($n = 5$ per group). (F) Macrophage infiltration in the eWAT of WT and *Cx3cr1*$^{-/-}$ mice fed the NC or HF diet at 20 weeks old, as evaluated by F4/80 immunostaining. Scale bar: 100 μm. (G)The ratio of F4/80-stained cells to total cells counted in eWAT of WT and *Cx3cr1*$^{-/-}$ mice fed on HF diet ($n = 4$ per group). (H) Adipocyte size of WT and *Cx3cr1*$^{-/-}$ mice fed the NC or HF diet ($n = 4$

**Table 2.** Effect of HF diet on metabolic parameter at 12 weeks

| | NC | | HF | |
|---|---|---|---|---|
| | WT | *Cx3cr1*$^{-/-}$ | WT | *Cx3cr1*$^{-/-}$ |
| Weight (g) | 27.0 ± 0.4 | 26.0 ± 0.4 | 40.0 ± 1.0 | 39.3 ± 0.8 |
| Liver weight (g) | 1.10 ± 0.02 | 1.03 ± 0.02 | 1.31 ± 0.14 | 1.16 ± 0.08 |
| eWAT weight (g) | 0.57 ± 0.05 | 0.70 ± 0.05 | 2.31 ± 0.13 | 2.37 ± 0.09 |
| Glucose (mg/mL) | 64.4 ± 6.1 | 71.6 ± 3.4 | 72.0 ± 8.7 | 115.8 ± 18.4 |
| TG (mg/dL) | 69.7 ± 13.7 | 109.4 ± 10.6* | 86.8 ± 10.6 | 105.3 ± 7.7 |
| Total cholesterol (mg/dL) | 113.78 ± 3.98 | 83.6 ± 3.9** | 183.0 ± 11.8 | 188.7 ± 15.4 |
| Nonesterified fatty acid (mEq/L) | 1.41 ± 0.3 | 2.1 ± 0.1 | 0.73 ± 0.08 | 0.85 ± 0.06 |

Date are means ± standard error and were obtained from 20 weeks old fasted *Cx3cr1*$^{-/-}$ mice and WT littermate controls ($n$ = 4-10 mice/group). *$P$ < 0.05, **$P$ < 0.01 *vs* WT on the same diet.

### Blockade of CCL2-CCR2 signaling in *Cx3cr1*$^{-/-}$ mice attenuates obesity-induced insulin resistance via M2 dominate shift in ATMs

There is accumulating evidence that CCL2-CCR2 is important for ATM recruitment and insulin resistance. We found that *Ccl2* and *Ccr2* expression was increased in the adipose tissue of *Cx3cr1*$^{-/-}$ mice in comparison with WT mice on the HF diet (Fig. 9A). To clarify the significance of CCL2-CCR2 and CX3CL1-CX3CR1 signaling in these processes, we generated *Ccl2* and *Cx3cr1* double knockout (DKO) mice by crossing *Ccl2*$^{-/-}$ mice with *Cx3cr1*$^{-/-}$ mice. DKO mice had similar body weights to their parental strains (Fig. 9B). However, HF diet-induced glucose intolerance and hyperinsulinemia in *Cx3cr1*$^{-/-}$ mice were improved by knockout of *Ccl2* (Fig. 9C and 9D).

To assess the effects of *Ccl2* deletion on ATM subsets in *Cx3cr1*$^{-/-}$ mice, we quantified M1 and M2 ATMs. The total number of ATMs was not different between genotypes on the same diet. However, DKO mice on the HF diet had 40% fewer M1 like macrophages and 91% more M2 like macrophages than WT mice, resulting in macrophage polarization toward an anti-inflammatory phenotype (Fig. 9E and 9F).

### Cx3cl1 protects against obesity-induced insulin resistance

The decreased levels of Cx3cl1 in the eWAT and plasma of DIO model of WT (DIO-WT) mice suggested that Cx3cl1 may exert therapeutic effects on obesity-induced insulin resistance and inflammation. Therefore, we expressed Cx3cl1 systemically in DIO-WT mice via hydrodynamic tail vein injection of the pLIVE- Cx3cl1 vector. Weight gain was unaffected by Cx3cl1 in DIO-WT mice (Fig. 10A). Systemic Cx3cl1 expression was sustained until 28 days (Fig. 10B). Meanwhile, Cx3cl1 tended to attenuate hyperinsulinemia in DIO-WT mice (Fig. 10C), which was negatively correlated with the insulin level (Fig. 10D) and attenuated glucose intolerance in DIO-WT (Fig. 10E). In addition, Cx3cl1-enhanced insulin signaling in both the liver and eWAT of DIO-WT mice (Fig. 10F). While there was no significant difference in hepatic steatosis or β cell mass between Cx3cl1-treated and control mice (Fig. 10G and 10H), the levels of *Ccl2* and *Tnf* mRNA expression were decreased in the liver of Cx3cl1-injected mice compared with control mice (Fig. 10I), while no alterations were observed in eWAT (Fig. 10J). However, in similar experiments in *Cx3cr1*$^{-/-}$ mice (Fig. 11A-11C) we found no significant improvement in glucose- intolerance (Fig. 11D) or hepatic steatosis (Fig. 11E and 11F). These results suggested that Cx3cl1 may have therapeutic effects on obesity-induced glucose intolerance and insulin sensitivity.

## Discussion

This study showed that CX3CL1-CX3CR1 signaling deficiency promoted obesity-induced inflammation and insulin resistance through polarization of M1 macrophages in eWAT. *Cx3cl1* mRNA expression was downregulated during the development of obesity. Furthermore, CX3CL1 and CX3CR1 were predominantly expressed

**Figure 2: continued**

per group). (I) mRNA expression of macrophage markers and TNF-α in eWAT from mice fed the NC or HF diet. Data were obtained from 20-week-old fasted *Cx3cr1*$^{-/-}$ mice, with WT littermates used as controls ($n$ = 5 per group). (J) Immunoblots of phosphorylated NF-κB p65 (p-NF-κB p65) and total proteins in the eWAT of mice. (K) Plasma TNF-α levels of WT and *Cx3cr1*$^{-/-}$ mice fed the NC or HF diet ($n$ = 5-6 per group). (L) Impaired insulin signaling in the liver and eWAT of *Cx3cr1*$^{-/-}$ mice fed the HF diet. Immunoblots of phospho-Tyr1146 insulin receptor β subunit (p-IRβ), IRβ, phospho-Ser473 Akt (p-Akt), Akt, and β-actin with or without intravenous insulin injection. The data in (C-E, G, I, and K) are expressed as means ± SEM and were compared using the 2-tailed Student's *t*-test; *$P$ < 0.05, **$P$ < 0.01, ***$P$ < 0.001.

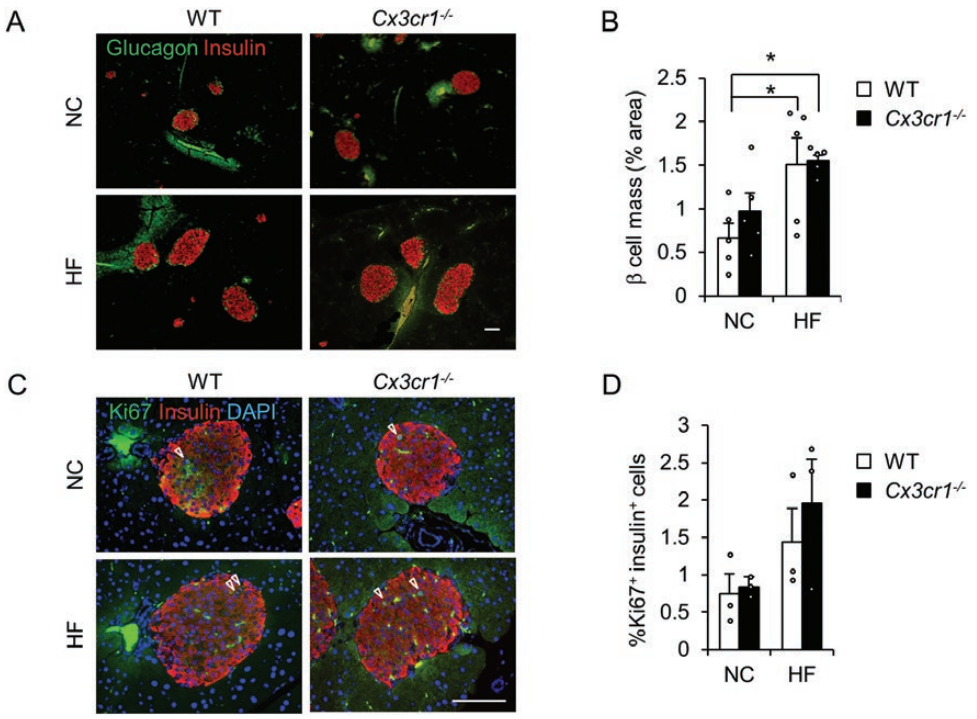


**Figure 3.** β cell mass and proliferation in *Cx3cl1*$^{-/-}$ mice. (A) Immunocytochemical analysis of the islets of mice fed the NC or HF diet using anti-insulin (red) and anti-glucagon (green) antibodies. Scale bar: 100 μm. (B) β cell masses of WT and *Cx3cr1–/–* mice fed the NC or HF diet ($n = 5$ per group). (C) Staining with anti-Ki67 (green) and anti-insulin (green) antibodies and 4′,6-diamidino-2-phenylindole. Arrows indicate Ki67$^+$ insulin$^+$ cells. Scale bar: 100 μm. (D) Percentages of Ki67$^+$ insulin$^+$ cells in pancreatic sections of WT and *Cx3cr1–/–* mice fed the NC or HF diet ($n = 3$ per group). The data in (B, D) are expressed as means ± SEM and were compared using the 2-tailed Student's *t*-test; $^*P < 0.05$.

in macrophages rather than adipocytes. CX3CR1 deficiency in DIO and *ob/ob* mice and in myeloid cells exacerbated adipose tissue inflammation and insulin resistance through a dynamic shift to an M1-dominant ATM phenotype. On the other hand, CCL2-CCR2 signaling deficiency in *Cx3cr1*$^{-/-}$ mice attenuated obesity-induced inflammation and insulin resistance. Interestingly, CX3CL1 treatment improved glucose tolerance and insulin sensitivity. These results indicated that CX3CL1-CX3CR1 signaling at least partially protected against diet-induced metabolic syndrome.

In previous studies, 2 polymorphisms (V249I and T280M) of human *CX3CR1* gene were shown to be associated with type 2 diabetes, metabolic syndrome, and Crohn's disease (18, 57, 58). For these polymorphisms, the binding affinity of CX3CL1 with its receptor was lower (59). Thus, CX3CL1-CX3CR1 signaling may be weakened in obese patients, contributing to the development of inflammatory diseases. However, the relationships of CX3CL1 level with the pathogenesis of obesity-induced inflammation and insulin resistance remained unclear. We showed that the plasma CX3CL1 level was negatively correlated with insulin level, and loss of CX3CL1-CX3CR1 signaling exacerbated adipose tissue inflammation and insulin resistance in both genetically (*ob/ob*) and diet-induced obese mice.

It has been reported that increased *Tnf* expression is likely to be directly related to an increase in ATM infiltration, as M1 macrophages are the primary source of TNF-α in obese adipose tissue (1, 60). Our study showed that the number of ATMs was increased in *Cx3cr1*$^{-/-}$ mice compared with WT mice on the HF diet and caused increases in the expression of proinflammatory cytokines and chemokines, such as *Tnf* and *Ccl2*, in DIO mice. In addition, these phenomena were associated with promotion of NF-κB p65. Activation of the TNF-α receptor stimulated NF-κB signaling via inhibition of IκB kinase and led to insulin resistance in *Cx3cr1*$^{-/-}$ mice.

We showed that Cx3cl1 and Cx3cr1 were predominantly expressed in macrophages rather than in adipocytes. Therefore, we next examined the significance of CX3CL1-CX3CR1 signaling in macrophages in the inflammatory response to obesity, by generating chimeric mice lacking Cx3cr1 only in myeloid cells derived from BMT. Cx3cr1-deficient myeloid cells alone were sufficient to promote HF diet-induced insulin resistance and fatty liver in association

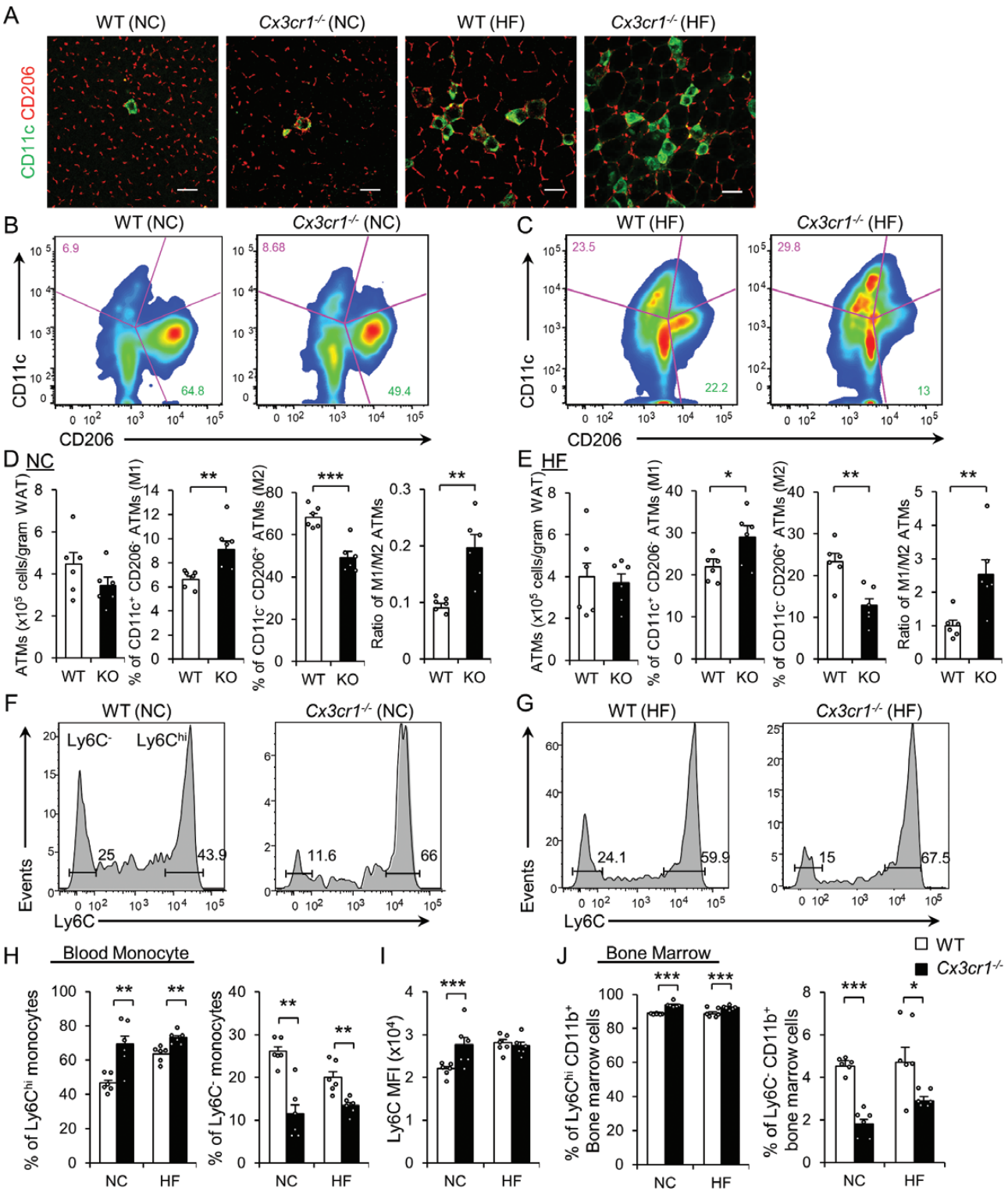


**Figure 4.** Increased M1-like and decreased M2-like macrophage expression in the eWAT of *Cx3cr1*$^{-/-}$ mice. (A) Representative immunostaining images using anti-CD11c (green) and anti-CD206 (red) antibodies in the eWAT of WT and *Cx3cr1*$^{-/-}$ mice fed the NC or HF diet at 16 weeks old. Scale bar: 100 μm. (B, C) CD11c$^{+}$ CD206$^{-}$ (M1-like) and CD11c$^{-}$ CD206$^{+}$ (M2-like) expression patterns in the ATMs of WT and *Cx3cr1*$^{-/-}$ mice fed the NC or HF diet. The representative results showed that the number of M1-like ATMs was increased, whereas the number of M2-like ATMs was decreased, in *Cx3cr1*$^{-/-}$ mice on both diets compared with WT mice. (D and E) Quantification of total ATMs and M1- and M2-like ATMs in the eWAT of mice fed the NC diet or HF diet ($n = 6$ per group). (F and G) Representative histograms showing the blood monocyte subsets (Ly6C$^{hi}$ and Ly6C$^{-}$) of mice fed the NC or HF diet for 8 weeks. (H and I) Quantitative analysis of Ly6C$^{hi}$ and Ly6C$^{-}$ blood monocytes of NC- or HF-diet-fed mice ($n = 6$ per group). Data are percentages of Ly6C$^{hi}$ and Ly6C$^{-}$ blood monocytes (H) and mean fluorescence intensity (MFI) of Ly6C in blood monocytes (I). (J) Data are the percentages of Ly6C$^{hi}$ and Ly6C$^{-}$ bone marrow cells. (K)The mRNA expression of macrophage markers and cytokines in peritoneal macrophages ($n = 6$ per group).The data in (D, E, H-J) are expressed as means ± SEM and were compared using the 2-tailed Student's *t*-test; $^{*}P < 0.05$, $^{**}P < 0.01$, $^{***}P < 0.001$.

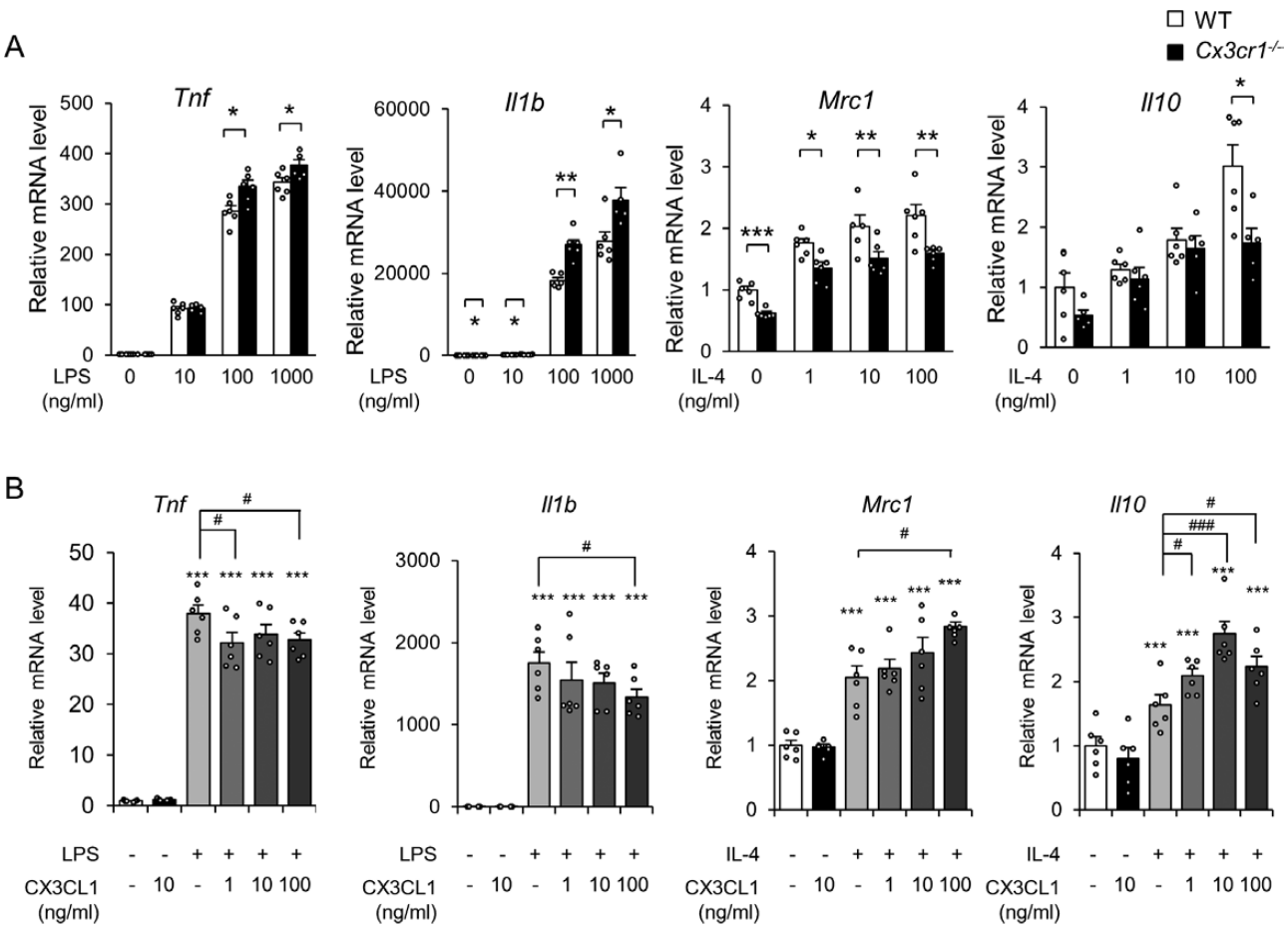


**Figure 5.** CX3CL1-CX3CR1 signaling suppresses LPS-induced M1 macrophage activation and enhances the expression of IL-4-induced M2 macrophage markers. (A) mRNA expression of macrophage markers and cytokines in peritoneal macrophages of WT and *Cx3cr1*$^{-/-}$ mice ($n = 6$ per group). (B) Peritoneal macrophages isolated from WT mice were co-incubated with 10 ng/mL LPS or 10 ng/mL IL-4 and 1 to 100 ng/mL Cx3cl1 for 16 h ($n = 4$-6 per treatment). The data of (A, B) are expressed as means ± SEM and were analyzed by 2-tailed Student's *t*-test; $^{*}P < 0.05$, $^{**}P < 0.01$, $^{***}P < 0.001$ *vs* the WT or control groups. $^{\#}P < 0.05$, $^{\#\#}P < 0.01$, $^{\#\#\#}P < 0.001$ *vs* the LPS- or IL-4-stimulated conditions.

with an increase in M1 macrophage filtration and a decrease in M2 macrophage filtration, thus recapitulating the metabolic and pathological phenotypes in *Cx3cr1*$^{-/-}$ mice. These observations indicated that CX3CL1-CX3CR1 signaling in myeloid cells is important in the development and maintenance of obesity-induced inflammation, fatty liver, and insulin resistance.

Recently, it was reported that the receptors Ccr2 and Cx3cr1 play key roles in determining the subsets of blood monocytes. Ccr2 is expressed in Ly6C$^{hi}$ inflammatory monocytes, which are recruited to inflamed tissues, while Cx3cr1 is expressed in resident monocytes (CCR2$^{-}$Ly6C$^{-}$) in noninflamed tissues (61, 62). Furthermore, CCR2$^{+}$Ly6C$^{hi}$ monocyte-derived macrophages can differentiate into an M1-like phenotype and CX3CR1$^{+}$Ly6C$^{-}$ monocytes generated M2-like macrophages in tissue (63). On the other hand, it has been reported that, on long-term HF diet administration, CX3CL1-CX3CR1 signaling was not associated with increased both Ly6C$^{hi}$ and Ly6C$^{low}$ monocytes but was required for Ly6C$^{low}$ monocyte survival (64). Our results showed that deficiency of CX3CL1-CX3CR1 signaling consistently increased the numbers of Ly6C$^{hi}$ monocytes and M1 macrophages and decreased the numbers of Ly6C$^{-}$ monocytes and M2 macrophages, in mice fed either the NC or HF diet for 8 weeks. These data suggested that CX3CL1-CX3CR1 signaling might be related to the determination of monocyte and macrophage subsets in early obesity. In addition, loss of macrophage CX3CR1 expression was associated with a stronger proinflammatory and weaker anti-inflammatory phenotype in the primary culture experiments. Furthermore, CX3CL1 inhibited LPS-induced M1-like polarization and promoted IL-4-induced M2-like polarization. CX3CL1-CX3CR1 signaling may be directly involved in macrophage polarization during the

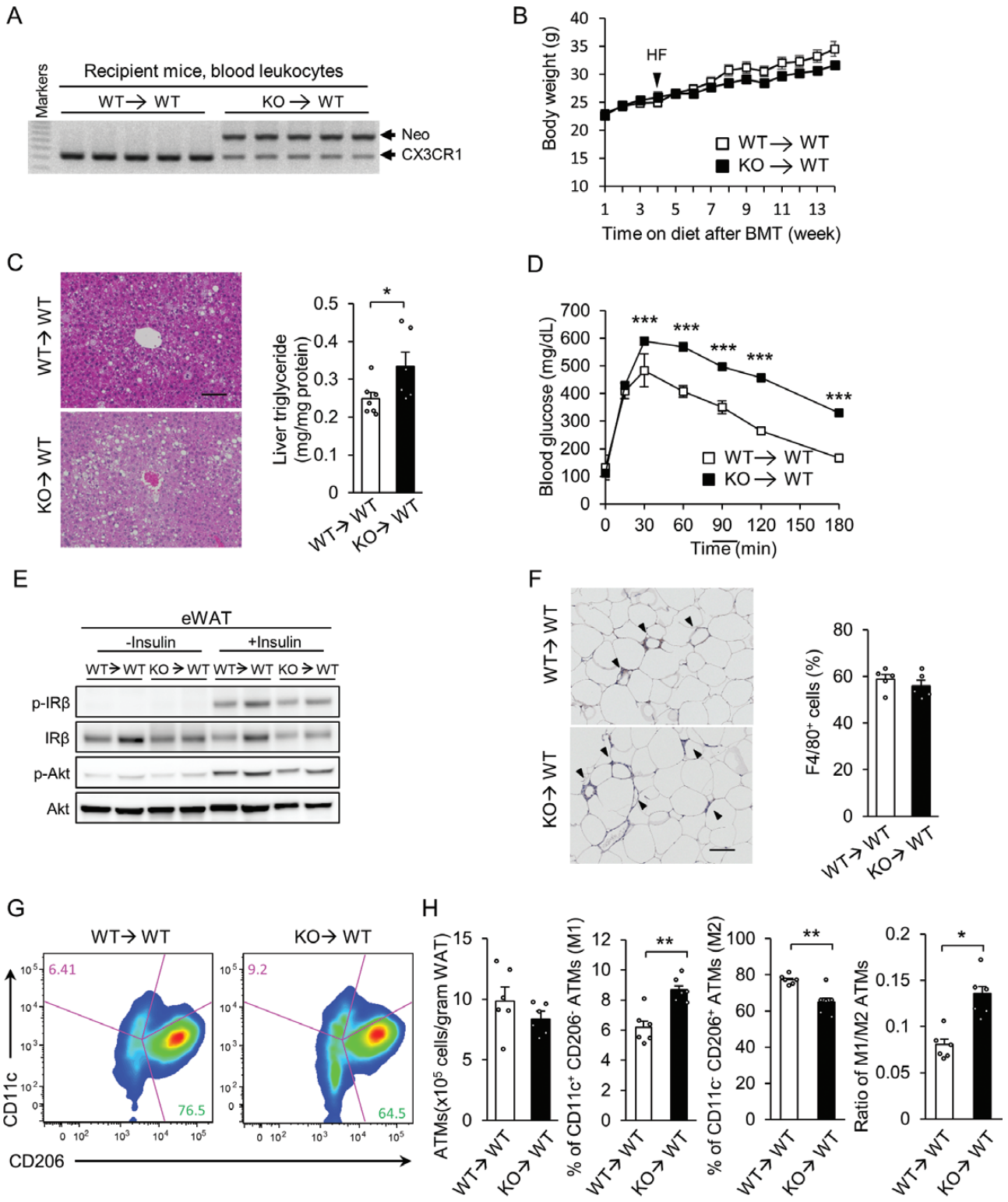


**Figure 6.** Chimeric mice lacking Cx3cr1 in myeloid cells show diet-induced insulin resistance, hepatic steatosis, and adipose tissue inflammation. (A) Expression of the Cx3cr1 deletion mutant *neo* gene was detected in peripheral blood leukocytes after BMT from KO to WT mice but not after BMT from WT to WT controls. (B) Weight gain of BMT recipient mice fed the HF diet for 9 weeks ($n = 6$ per group). (C) Representative images of HE stained of the liver and hepatic TG content ($n = 6$ per group). Scale bar: 100 μm. (D) GTT results of BMT mice fed the HF diet for 8 weeks ($n = 6$ per group). (E) Impaired insulin signaling in the eWAT of KO to WT mice fed the HF diet. (F) Macrophage infiltration of eWAT after KO to WT and WT to WT transplantation in mice fed an HF diet at 9 weeks, as evaluated by F4/80 immunostaining. Scale bar: 100 μm. (G) Representative results show that M1-like ATMs were increased, whereas M2-like ATMs were decreased in KO to WT mice fed the HF diet compared with WT mice. (H) Quantification of M1- and M2-like ATMs in the eWAT of mice fed the HF diet for 6 weeks ($n = 6$ per group). Data were ATM counts normalized relative to cell number and epididymal fat weight and percentages of M1- and M2-like ATMs. The data in (C, D, F, and H) are expressed as means ± SEM and were compared using the 2-tailed Student's *t*-test; $^{*}P < 0.05$, $^{**}P < 0.01$, $^{***}P < 0.001$.

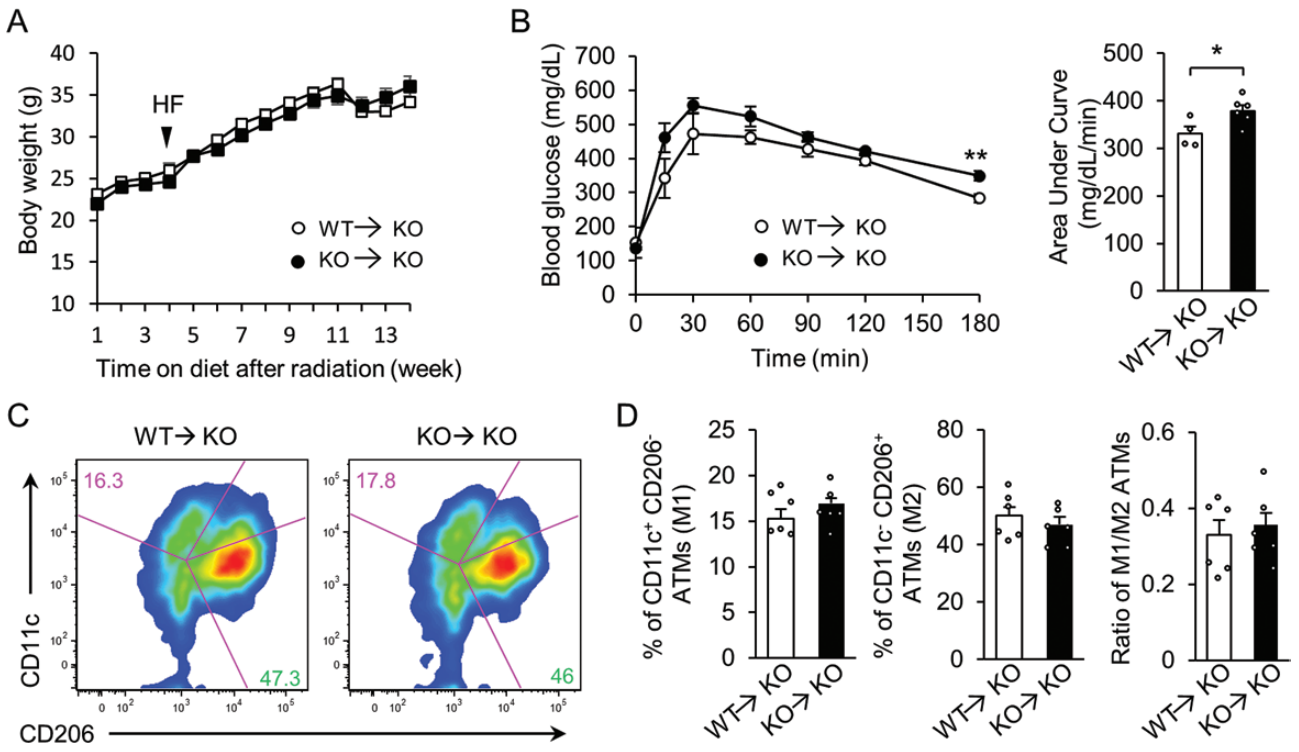


**Figure 7.** Phenotype of Cx3cr1 expression myeloid cells in *Cx3cr1*$^{-/-}$ mice. (A) Weight gains of the WT to KO and KO to KO mice fed an HF diet for 10 weeks after BMT (n = 6 per group). (B) GTT results for BMT mice fed an HF diet for 8 weeks (n = 4-6 per group). (C) Representative plots revealing M1- and M2-like ATMs in KO to KO mice and WT to KO mice. (D) Quantitation of M1- and M2-like ATMs in the WAT of mice fed the HF diet for 6 weeks (n = 6 per group). The data are the percentages of M1- and M2-like ATMs. The data in (B) are expressed as means ± SEM and were analyzed by 2-tailed Student's *t*-test; **P* < 0.05.

development of obesity. On the other hand, CCL2-CCR2 signaling deficit in *Cx3cr1*$^{-/-}$ mice was shown to decrease the numbers of M1 macrophages and increase the numbers of M2 macrophages compared with *Cx3cr1*$^{-/-}$ mice on the HF diet, thereby enhancing insulin sensitivity in *Ccl2* and *Cx3cr1* DKO mice. Thus, CX3CL1-CX3CR1 signaling and CCL2-CCR2 signaling may independently regulate M1/M2 polarization and contribute reciprocally to obesity-induced inflammation and insulin resistance. It will be interesting to more thoroughly explore whether the Cx3cl1 axis is further connected to Ccl2.

Our data demonstrated that in vivo overexpression of Cx3cl1 attenuated glucose- intolerance and enhanced insulin-sensitivity in both the liver and eWAT of DIO mice. Furthermore, the levels of proinflammatory cytokines were downregulated in the liver but not in eWAT. This phenomenon occurred only in the liver because hydrodynamic tail vein injection induces the expression of exogenous proteins in hepatocytes (65). Although hepatic steatosis was unaffected by Cx3cl1 treatment in our study, prolonged exposure to Cx3cl1 (28 days) may exert some protective effects. However, an increase in the plasma Cx3cl1 level had no effect on insulin sensitivity in *Cx3cr1*$^{-/-}$ mice, suggesting that the protective effect of Cx3cl1 was mediated by its receptor. Therefore, the CX3CL1-CX3CR1 signaling may be a target for the treatment of obesity and type 2 diabetes.

CX3CL1-CX3CR1 signaling plays a role in glycemic control by regulating insulin secretion in the context of β cell function, and Cx3cl1 treatment reverses β cell abnormalities (20, 66). Our study showed that β cell mass increased in mice on the HF diet compared with the NC diet but did not differ according to genotype or with Cx3cl1 overexpression. Moreover, CX3CL1-CX3CR1 signaling had no effect on β cell proliferation. While hyperinsulinemia was attenuated by Cx3cl1, our data indicated that the functional profile of Cx3cl1 may be related to improved insulin sensitivity, rather than the regulation of β cell secretory function. Furthermore, CX3CL1-CX3CR1 signaling in female mice positively regulates the metabolic phenotype via hypothalamic microglial activation (21). As we used male mice in the present study, microglial Cx3cr1 signaling would have had no effect on metabolic phenotype. We plan to perform a detailed analysis of hypothalamic microglial activation in *Cx3cr1*$^{-/-}$ male mice.

In summary, our findings suggested that CX3CL1-CX3CR1 signaling plays a critical role in obesity-induced

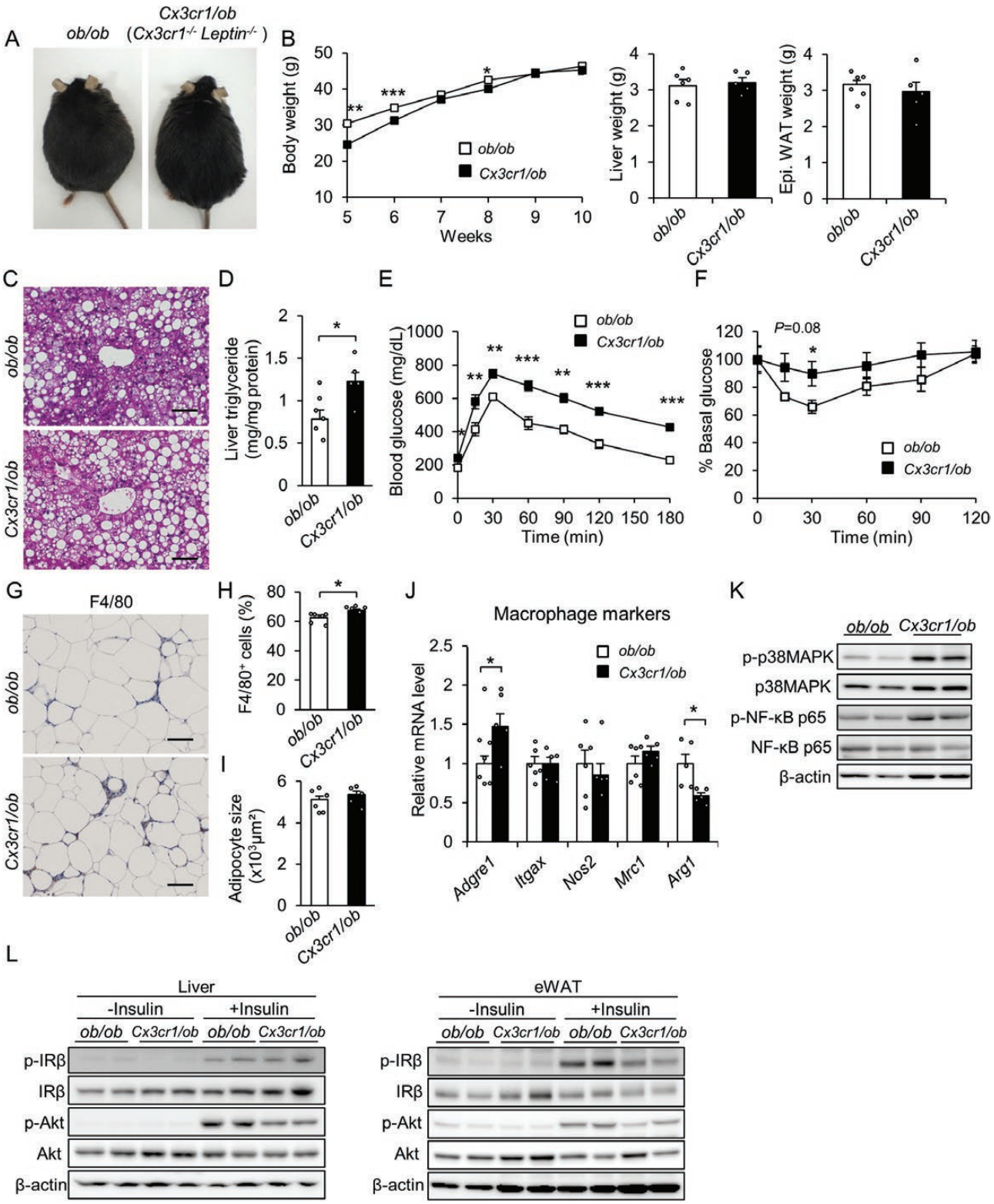


**Figure 8.** Cx3cr1 deficiency in *ob/ob* mice promotes insulin resistance, hepatic steatosis, and adipose tissue inflammation. (A) Generation of *Cx3cr1/ob* (*Cx3cr1*$^{-/-}$ *Leptin*$^{-/-}$) mice. (B) Weight gain of control (*ob/ob*) and *Cx3cr1/ob* mice ($n$ = 5-6 per group) at 10 weeks old. (C) Representative images of HE-stained slides of the liver. Scale bar: 100 μm. (D) HepaticTG content ($n$ = 5-6 per group). (E) GTT ($n$ = 5-6 per group). (F) Plasma insulin levels of *ob/ob* and *Cx3cr1/ob* mice in the fasted or fed state ($n$ = 5-6 per group). (G) Macrophage infiltration in the eWAT of *ob/ob* and *Cx3cr1/ob* mice at 10 weeks old as evaluated by F4/80 immunostaining. Scale bar: 100 μm. (H) Ratio of F4/80-positive cells to total cells counted in the eWAT ($n$ = 3-4 per group). (I) Adipocyte size of *ob/ob* and *Cx3cr1/ob* mice ($n$ = 3-4 per group). (J) mRNA expression of macrophage markers in eWAT from *ob/ob* and *Cx3cr1/ob* mice ($n$ = 5-6 per group). (K) Exacerbation of inflammatory signaling in the eWAT of *Cx3cr1/ob* mice. Immunoblotting analysis of p-p38MAPK, p-NF-κB p65, and their total proteins in eWAT. (L) Impaired insulin signaling in the liver and eWAT of *Cx3cr1/ob* mice. Immunoblots of phospho-Tyr1146 insulin receptor β subunit (p-IRβ), IRβ, phospho-Ser473 Akt (p-Akt), and Akt in the liver and eWAT of *ob/ob* or *Cx3cr1/ob* mice. The data of (D-F, H, and J) are expressed as means ± SEM and were compared using the 2-tailed Student's *t*-test; *$P < 0.05$, **$P < 0.01$, ***$P < 0.001$.

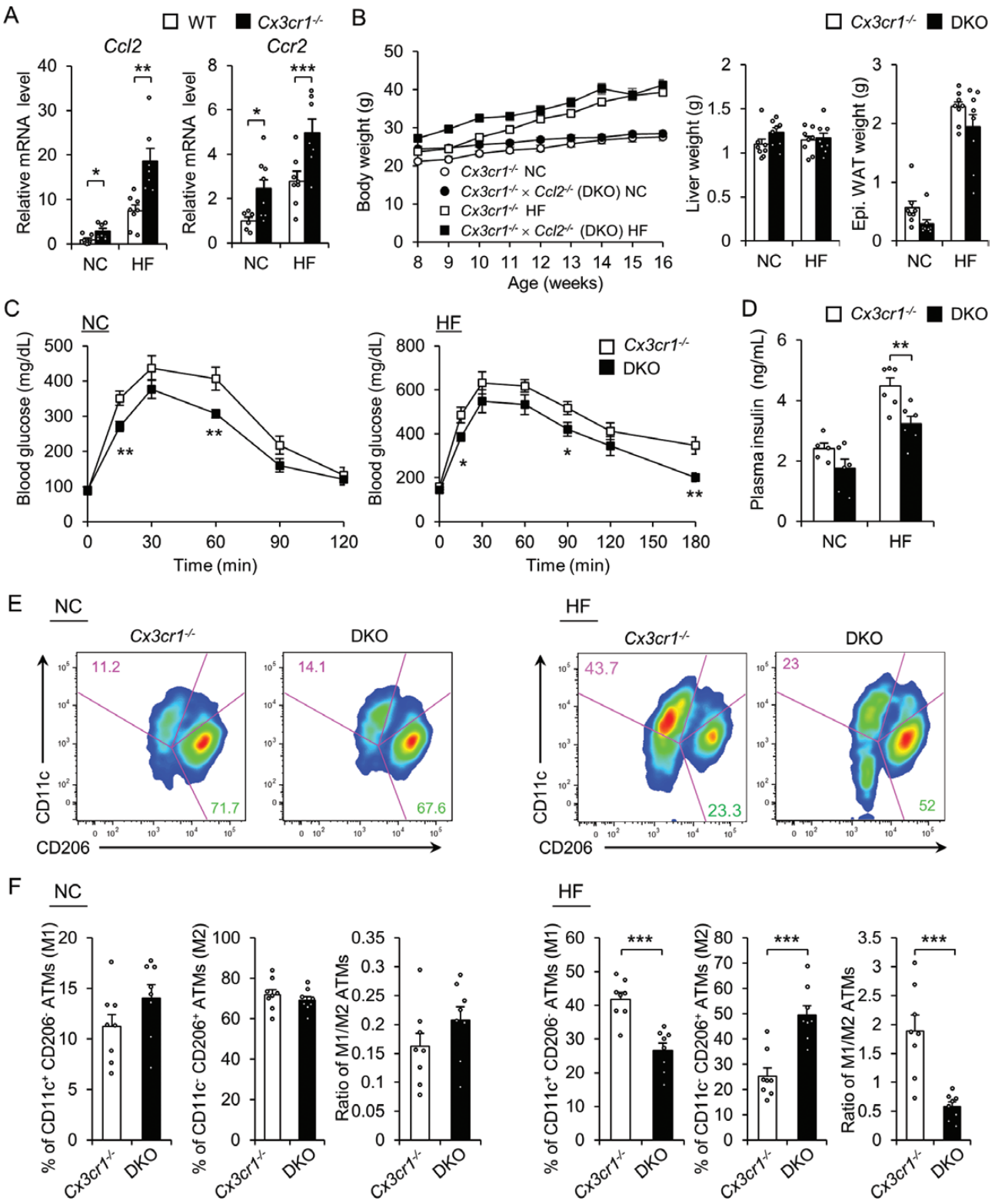


**Figure 9.** *Ccl2* deficiency in *Cx3cr1*$^{-/-}$ mice attenuates insulin resistance and adipose inflammation via a significant reduction in the M1/M2 ratio. (A) mRNA expression of *Ccl2* and *Ccr2* in eWAT from mice fed the NC or HF diet. Data were obtained from 20-week-old fasted *Cx3cr1*$^{-/-}$ mice and WT littermate controls ($n = 6$-8 per group). (B) The body and tissue weights of *Cx3cr1*$^{-/-}$ and *Cx3cr1*$^{-/-}$ × *Ccl2*$^{-/-}$ (DKO) mice fed the NC or HF diet for 16 weeks ($n = 8$ per group). (C) GTT ($n = 5$-6 per group). (D) Plasma insulin levels in the fed state ($n = 5$-6 per group). (E) Representative results showing that M1-like ATMs were decreased, whereas M2-like ATMs were increased in DKO mice fed the HF diet compared with *Cx3cr1*$^{-/-}$ mice. (F) Quantification of M1- and M2-like ATMs in the eWAT of mice fed the NC diet or HF diet for 16 weeks ($n = 8$ per group). Data are percentages of M1- and M2-like ATMs. Data in (A, C, D, and F) are expressed as means ± SEM and were analyzed by 2-tailed Student's *t*-test; $^{*}P < 0.05$, $^{**}P < 0.01$, $^{***}P < 0.001$.

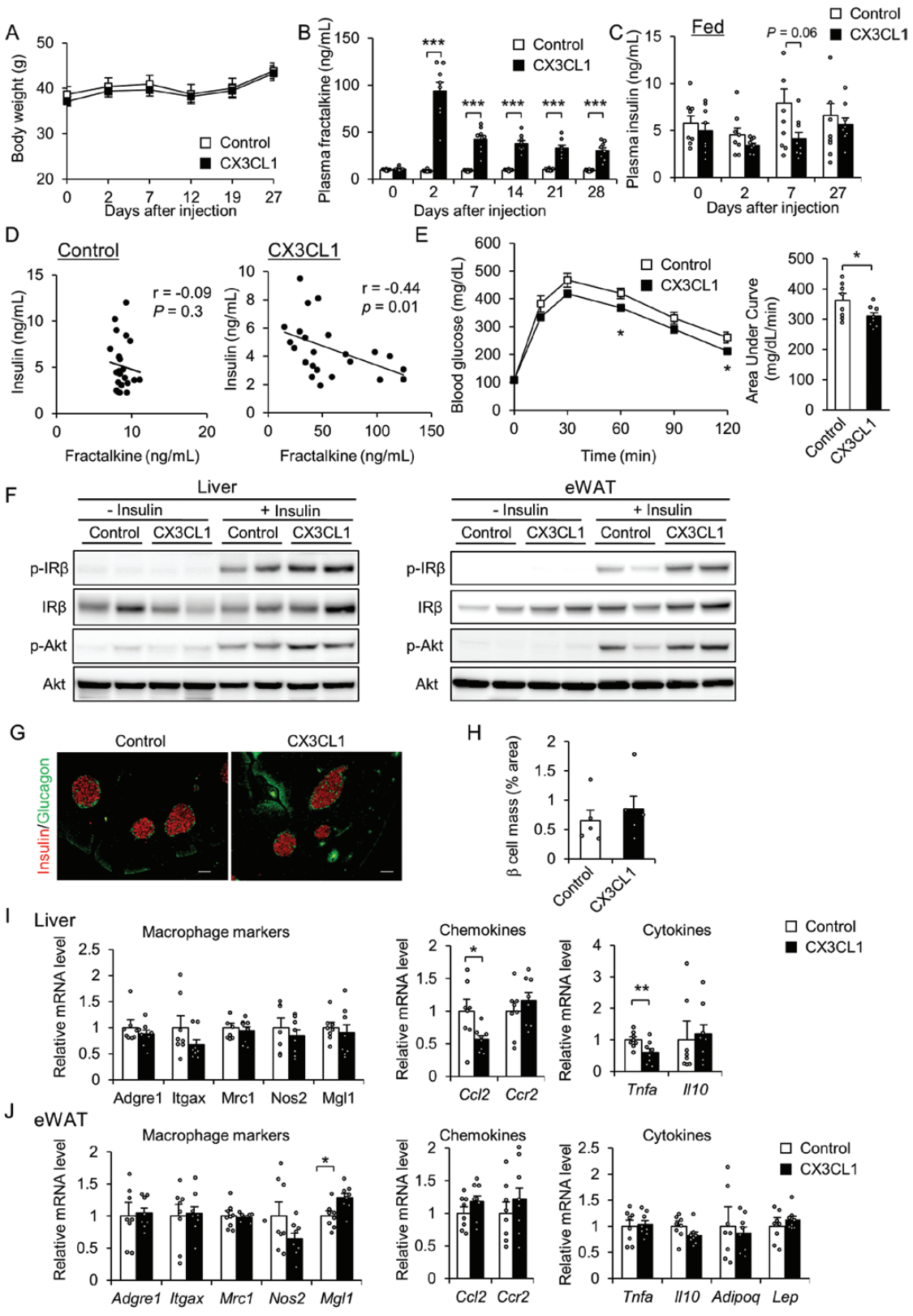


**Figure 10.** Cx3cl1 treatment enhances diet-induced insulin sensitivity. (A) Weight gain of DIO-WT mice after hydrodynamic injection of pLIVE empty vector (control) or pLIVE-CX3CL1 from 0 to 27 days ($n = 8$ per group). (B) Time course of changes in Cx3cl1 expression in plasma after hydrodynamic injection ($n = 8$ per group). (C) Time course of changes in plasma insulin levels after hydrodynamic injection ($n = 8$ per group). (D) Correlation of plasma insulin with Cx3cl1 after hydrodynamic injection of control or Cx3cl1 ($n = 24$-26). (E) GTT results of DIO-WT mice after 14 days with hydrodynamic injection of control or Cx3cl1 ($n = 8$ per group). (F) Enhanced insulin signaling in the liver and eWAT after hydrodynamic injection of Cx3cl1.

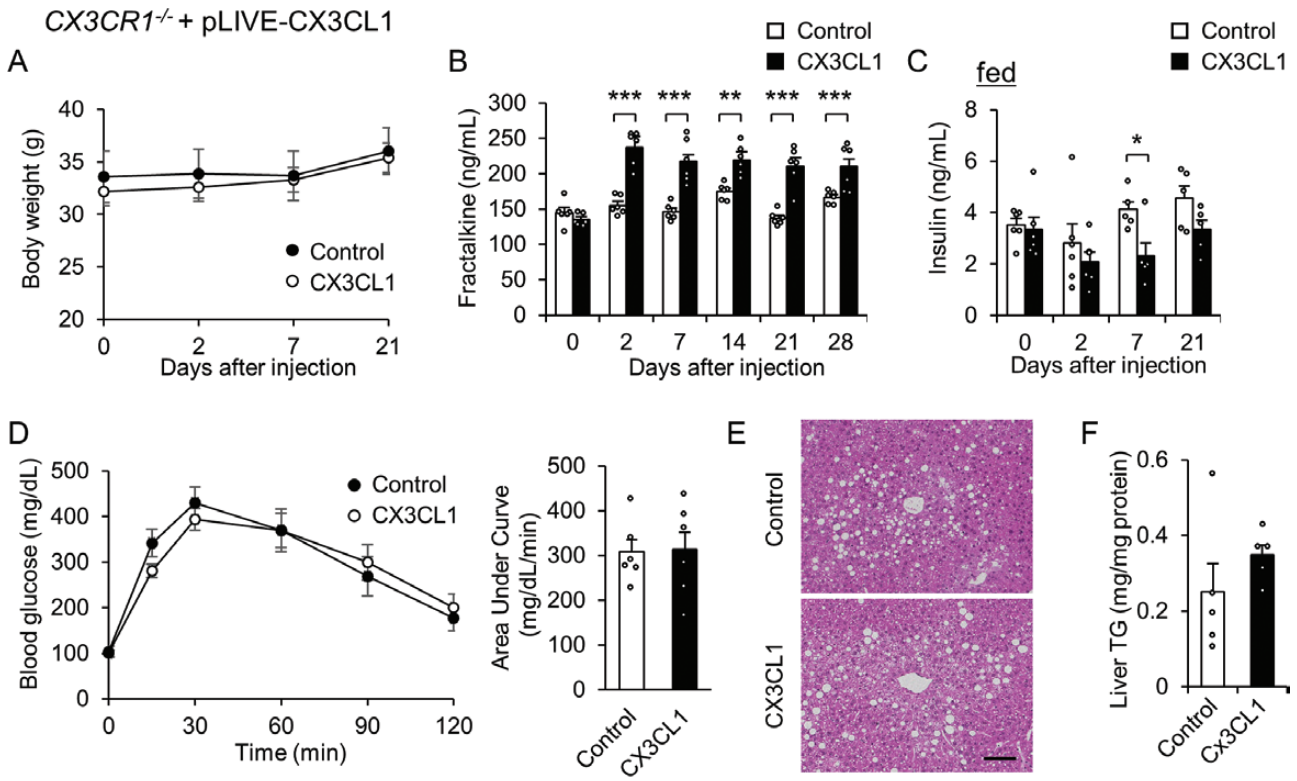


**Figure 11.** Cx3cl1 treatment has no effect on diet-induced insulin resistance in *Cx3cr1*$^{-/-}$ mice. (A) The weight gain of *Cx3cr1*$^{-/-}$ mice after hydrodynamic injection of the pLIVE empty vector (control) or pLIVE-CX3CL1 vector (CX3CL1) from days 0 to 21 ($n = 6$ per group). (B) The time course of Cx3cl1 expression in plasma after hydrodynamic injection ($n = 6$ per group). (C) The time course of the plasma insulin level after hydrodynamic injection ($n = 5$-6 per group). (D) GTT results after 14 days of hydrodynamic injection of the control or Cx3cl1 ($n = 6$ per group). (E) Representative images of HE-stained liver slices. Scale bar: 100 μm. (F) Hepatic TG content ($n = 5$ per group). Data in (B and C) are expressed as means ± SEM and were analyzed by 2-tailed Student's *t*-test; $^{*}P < 0.05$, $^{**}P < 0.01$, $^{***}P < 0.001$.

inflammation and insulin resistance by regulating the M1/M2 status of macrophages. Loss of CX3CL1-CX3CR1 signaling results in macrophage polarization toward an anti-inflammatory phenotype, thereby negatively regulating obesity-induced insulin resistance, diabetes, and nonalcoholic fatty liver disease. Overall, our study highlighted the potential clinical utility of the CX3CL1-CX3CR1 system for improving type 2 diabetes.

## Acknowledgments

The authors thank M. Nakayama and K. Hara (Kanazawa University, Japan) for technical assistance and animal care.

*Financial Support:* This work was supported by a Grant-in-Aid for Scientific Research (C) from MEXT, Japan (grant number 19K11764).

*Author Contributions:* MN conceived the study and wrote the manuscript; MN, KS, YN, NN, and LX performed experiments and collected and analyzed data; MK performed DNA microarray analysis; NM provided Cx3cr1 knockout mice and CCL2 knockout mice; KS, YN, TO, TY, and SK contributed to discussions and edited the manuscript; and MN supervised and delivered the project and acquired funding. All authors reviewed the manuscript.

## Additional Information

*Correspondence*: Mayumi Nagashimada, PhD, Assistant Professor, Division of Health Sciences, Kanazawa University Graduate School of Medical Science, Kanazawa, 920-0942, Japan. E-mail: nakanaga@staff.kanazawa-u.ac.jp.

*Disclosures:* The authors have nothing to disclose and no potential conflicts of interest relevant to this article to report.

*Data Availability:* All data generated or analyzed during this study are included in this published article or in the data repositories listed in references.

**Figure 10: continued**

Immunoblots of phospho-Tyr1146 insulin receptor β subunit (p-IRβ), IRβ, phospho-Ser473 Akt (p-Akt), and Akt. (G) Immunocytochemical analysis in the islets of control or CX3CL1 mice using anti-insulin (red) and antiglucagon (green) antibodies. Scale bar: 100 μm. (H) β cell masses in control and CX3CL1 mice. Means ± SEM ($n = 5$ per group). (I and J) mRNA expression of macrophage markers, chemokines, and cytokines in the liver and eWAT after hydrodynamic injection of control or CX3CL1 ($n = 8$ per group)The data of (B, C, E, and H-J) are expressed as means ± SEM and were compared using the 2-tailed Student's *t*-test; $^{*}P < 0.05$, $^{**}P < 0.01$, $^{***}P < 0.001$.

## References


1. Xu H, Barnes GT, Yang Q, et al. Chronic inflammation in fat plays a crucial role in the development of obesity-related insulin resistance. *J Clin Invest*. 2003;**112**(12):1821-1830.
2. Hotamisligil GS. Inflammation and metabolic disorders. *Nature*. 2006;**444**(7121):860-867.
3. Kanda H, Tateya S, Tamori Y, et al. MCP-1 contributes to macrophage infiltration into adipose tissue, insulin resistance, and hepatic steatosis in obesity. *J Clin Invest*. 2006;**116**(6):1494-1505.
4. Ota T. Chemokine systems link obesity to insulin resistance. *Diabetes Metab J*. 2013;**37**(3):165-172.
5. Kitade H, Sawamoto K, Nagashimada M, et al. CCR5 plays a critical role in obesity-induced adipose tissue inflammation and insulin resistance by regulating both macrophage recruitment and M1/M2 status. *Diabetes*. 2012;**61**(7):1680-1690.
6. Ota T. CCR5: A novel player in the adipose tissue inflammation and insulin resistance? *Adipocyte*. 2013;**2**(2):99-103.
7. Imai T, Hieshima K, Haskell C, et al. Identification and molecular characterization of fractalkine receptor CX3CR1, which mediates both leukocyte migration and adhesion. *Cell*. 1997;**91**(4):521-530.
8. Landsman L, Bar-On L, Zernecke A, et al. CX3CR1 is required for monocyte homeostasis and atherogenesis by promoting cell survival. *Blood*. 2009;**113**(4):963-972.
9. Fong AM, Robinson LA, Steeber DA, et al. Fractalkine and CX3CR1 mediate a novel mechanism of leukocyte capture, firm adhesion, and activation under physiologic flow. *J Exp Med*. 1998;**188**(8):1413-1419.
10. Zernecke A, Shagdarsuren E, Weber C. Chemokines in atherosclerosis: an update. *Arterioscler Thromb Vasc Biol*. 2008;**28**(11):1897-1908.
11. Tacke F, Alvarez D, Kaplan TJ, et al. Monocyte subsets differentially employ CCR2, CCR5, and CX3CR1 to accumulate within atherosclerotic plaques. *J Clin Invest*. 2007;**117**(1):185-194.
12. Combadière C, Potteaux S, Gao JL, et al. Decreased atherosclerotic lesion formation in CX3CR1/apolipoprotein E double knockout mice. *Circulation*. 2003;**107**(7):1009-1016.
13. Apostolakis S, Spandidos D. Chemokines and atherosclerosis: focus on the CX3CL1/CX3CR1 pathway. *Acta Pharmacol Sin*. 2013;**34**(10):1251-1256.
14. McDermott DH, Fong AM, Yang Q, et al. Chemokine receptor mutant CX3CR1-M280 has impaired adhesive function and correlates with protection from cardiovascular disease in humans. *J Clin Invest*. 2003;**111**(8):1241-1250.
15. Nanki T, Imai T, Nagasaka K, et al. Migration of CX3CR1-positive T cells producing type 1 cytokines and cytotoxic molecules into the synovium of patients with rheumatoid arthritis. *Arthritis Rheum*. 2002;**46**(11):2878-2883.
16. Ruth JH, Volin MV, Haines GK 3rd, et al. Fractalkine, a novel chemokine in rheumatoid arthritis and in rat adjuvant-induced arthritis. *Arthritis Rheum*. 2001;**44**(7):1568-1581.
17. Yang J, Zhang L, Yu C, Yang XF, Wang H. Monocyte and macrophage differentiation: circulation inflammatory monocyte as biomarker for inflammatory diseases. *Biomark Res*. 2014;**2**(1):1.
18. Leonardi I, Li X, Semon A, et al. CX3CR1+ mononuclear phagocytes control immunity to intestinal fungi. *Science*. 2018;**359**(6372):232-236.
19. Medina-Contreras O, Geem D, Laur O, et al. CX3CR1 regulates intestinal macrophage homeostasis, bacterial translocation, and colitogenic Th17 responses in mice. *J Clin Invest*. 2011;**121**(12):4787-4795.
20. Lee YS, Morinaga H, Kim JJ, et al. The fractalkine/CX3CR1 system regulates β cell function and insulin secretion. *Cell*. 2013;**153**(2):413-425.
21. Dorfman MD, Krull JE, Douglass JD, et al. Sex differences in microglial CX3CR1 signalling determine obesity susceptibility in mice. *Nat Commun*. 2017;**8**:14556.
22. Ishida Y, Kuninaka Y, Yamamoto Y, et al. Pivotal involvement of the CX3CL1-CX3CR1 axis for the recruitment of M2 tumor-associated macrophages in skin carcinogenesis. *J Invest Dermatol*. 2020;140(10):1951-1961.e6.
23. Lu P, Li L, Kuno K, et al. Protective roles of the fractalkine/CX3CL1-CX3CR1 interactions in alkali-induced corneal neovascularization through enhanced antiangiogenic factor expression. *J Immunol*. 2008;**180**(6):4283-4291.
24. Ni Y, Nagashimada M, Zhuge F, et al. Astaxanthin prevents and reverses diet-induced insulin resistance and steatohepatitis in mice: a comparison with vitamin E. *Sci Rep*. 2015;**5**:17192.
25. Ni Y, Nagashimada M, Zhan L, et al. Prevention and reversal of lipotoxicity-induced hepatic insulin resistance and steatohepatitis in mice by an antioxidant carotenoid, β-cryptoxanthin. *Endocrinology*. 2015;**156**(3):987-999.
26. RRID:AB_2811268. http://antibodyregistry.org/AB_2811268
27. RRID:AB_2890095. http://antibodyregistry.org/AB_2890095
28. RRID:AB_2575663. http://antibodyregistry.org/AB_2575663
29. RRID:AB_331641. http://antibodyregistry.org/AB_331641
30. RRID:AB_330713. http://antibodyregistry.org/AB_330713
31. RRID:AB_331284. https://scicrunch.org/resolver/AB_331284
32. RRID:AB_330561. https://scicrunch.org/resolver/AB_330561
33. RRID:AB_331578. https://scicrunch.org/resolver/AB_331578
34. RRID:AB_2280448. 8. https://scicrunch.org/resolver/AB_2280448
35. RRID:AB_329825. https://scicrunch.org/resolver/AB_329825
36. RRID:AB_329827. https://scicrunch.org/resolver/AB_329827
37. RRID:AB_476744. https://scicrunch.org/resolver/AB_476744
38. RRID:AB_1140040. http://antibodyregistry.org/AB_1140040
39. RRID:AB_306130. http://antibodyregistry.org/AB_306130
40. RRID:AB_259852. http://antibodyregistry.org/AB_259852
41. RRID:AB_443209. http://antibodyregistry.org/AB_443209
42. Lumeng CN, DelProposto JB, Westcott DJ, Saltiel AR. Phenotypic switching of adipose tissue macrophages with obesity is generated by spatiotemporal differences in macrophage subtypes. *Diabetes*. 2008;**57**(12):3239-3246.
43. RRID:AB_306203. http://antibodyregistry.org/AB_306203
44. RRID:AB_10891146. http://antibodyregistry.org/AB_10891146
45. RRID:AB_322613. http://antibodyregistry.org/AB_322613
46. RRID:AB_324695. http://antibodyregistry.org/AB_324695
47. RRID:AB_1288416. http://antibodyregistry.org/AB_1288416
48. RRID:AB_2313584. http://antibodyregistry.org/AB_2313584
49. RRID:AB_138404. http://antibodyregistry.org/AB_138404
50. RRID:AB_2338997. http://antibodyregistry.org/AB_2338997
51. RRID:AB_10561522. http://antibodyregistry.org/AB_10561522
52. RRID:AB_2338999. http://antibodyregistry.org/AB_2338999
53. RRID:AB_2340474. http://antibodyregistry.org/AB_2340474
54. Zhuge F, Ni Y, Nagashimada M, et al. DPP-4 inhibition by linagliptin attenuates obesity-related inflammation and insulin

resistance by regulating M1/M2 macrophage polarization. *Diabetes*. 2016;**65**(10):2966-2979.
55. Cho KW, Morris DL, Lumeng CN. Flow cytometry analyses of adipose tissue macrophages. *Methods Enzymol*. 2014;**537**:297-314.
56. Sasaki S, Baba T, Shinagawa K, Matsushima K, Mukaida N. Crucial involvement of the CCL3-CCR5 axis-mediated fibroblast accumulation in colitis-associated carcinogenesis in mice. *Int J Cancer*. 2014;**135**(6):1297-1306.
57. Shah R, Hinkle CC, Ferguson JF, et al. Fractalkine is a novel human adipochemokine associated with type 2 diabetes. *Diabetes*. 2011;**60**(5):1512-1518.
58. Sirois-Gagnon D, Chamberland A, Perron S, Brisson D, Gaudet D, Laprise C. Association of common polymorphisms in the fractalkine receptor (CX3CR1) with obesity. *Obesity (Silver Spring)*. 2011;**19**(1):222-227.
59. Faure S, Meyer L, Costagliola D, et al. Rapid progression to AIDS in HIV+ individuals with a structural variant of the chemokine receptor CX3CR1. *Science*. 2000;**287**(5461):2274-2277.
60. Weisberg SP, McCann D, Desai M, Rosenbaum M, Leibel RL, Ferrante AW Jr. Obesity is associated with macrophage accumulation in adipose tissue. *J Clin Invest*. 2003;**112**(12):1796-1808.
61. Geissmann F, Jung S, Littman DR. Blood monocytes consist of two principal subsets with distinct migratory properties. *Immunity*. 2003;**19**(1):71-82.
62. Geissmann F, Auffray C, Palframan R, et al. Blood monocytes: distinct subsets, how they relate to dendritic cells, and their possible roles in the regulation of T-cell responses. *Immunol Cell Biol*. 2008;**86**(5):398-408.
63. Italiani P, Boraschi D. From monocytes to M1/M2 macrophages: phenotypical vs. functional differentiation. *Front Immunol*. 2014;**5**:514.
64. Morris DL, Oatmen KE, Wang T, DelProposto JL, Lumeng CN. CX3CR1 deficiency does not influence trafficking of adipose tissue macrophages in mice with diet-induced obesity. *Obesity (Silver Spring)*. 2012;**20**(6):1189-1199.
65. Liu F, Song Y, Liu D. Hydrodynamics-based transfection in animals by systemic administration of plasmid DNA. *Gene Ther*. 1999;**6**(7):1258-1266.
66. Riopel M, Seo JB, Bandyopadhyay GK, et al. Chronic fractalkine administration improves glucose tolerance and pancreatic endocrine function. *J Clin Invest*. 2018;**128**(4):1458-1470.